Atmospheric
Chemistry
and Physics
Discussions

Open Access

Turbulence Kinetic Energy budget during the afternoon transition – Part 2: A simple TKE model

E. Nilsson[1,2], M. Lothon[1], F. Lohou[1], E. Pardyjak[3], O. Hartogensis[4], and C. Darbieu[1]

[1]Laboratoire d'Aerologie, University of Toulouse, CNRS, Toulouse, France
[2]Department of Earth Sciences, Uppsala University, Uppsala, Sweden
[3]Department of Mechanical Engineering, Utah University, Salt Lake City, UT, USA
[4]Meteorology and Air Quality Section, Wageningen University, Wageningen, the Netherlands

Discussion Paper | Discussion Paper | Discussion Paper | Discussion Paper |

ACPD

15, 29807–29869, 2015

A simple TKE model

E. Nilsson et al.

Title Page

Abstract   Introduction

Conclusions   References

Tables   Figures

◄   ►

◄   ►

Back   Close

Full Screen / Esc

Printer-friendly Version

Interactive Discussion

Abstract

A simple model for turbulence kinetic energy (TKE) and the TKE budget is presented for sheared convective atmospheric conditions based on observations from the Boundary Layer Late Afternoon and Sunset Turbulence (BLLAST) field campaign. It is based
5 on an idealized mixed-layer approximation and a simplified near-surface TKE budget. In this model, the TKE is dependent on four budget terms (turbulent dissipation rate, buoyancy production, shear production and vertical transport of TKE) and only requires measurements of three input available (near-surface buoyancy flux, boundary layer depth and wind speed at one height in the surface layer).

10 This simple model is shown to reproduce some of the observed variations between the different studied days in terms of near-surface TKE and its decay during the afternoon transition reasonably well. It is subsequently used to systematically study the effects of buoyancy and shear on TKE evolution using idealized constant and time-varying winds during the afternoon transition. From this, we conclude that many
15 different TKE decay rates are possible under time-varying winds and that generalizing the decay with simple scaling laws for near-surface TKE of the form t^α may be questionable.

The model's errors result from the exclusion of processes such as elevated shear production and horizontal advection. The model also produces an overly rapid decay
20 of shear production with height. However, the most influential budget terms governing near-surface TKE in the observed sheared convective boundary layers are included, while only second order factors are neglected. Comparison between modeled and averaged observed estimates of dissipation rate illustrate that the overall behavior of the model is often quite reasonable. Therefore, we use the model to discuss the low
25 turbulence conditions that form first in the upper parts of the boundary layer during the afternoon transition and are only apparent later near the surface. This occurs as a consequence of the continuous decrease of near-surface buoyancy flux during the afternoon transition. This region of weak afternoon turbulence is hypothesized to be a

"pre-residual layer," which is important in determining the onset conditions for the weak sporadic turbulence that occur in the residual layer once near-surface stratification has become stable.

1   Introduction

The daytime atmospheric boundary layer (ABL) is characterized by unstable stratification, turbulent mixing of momentum, heat, scalars and buoyancy-driven eddies. These large eddies are generated by a strong surface heat flux (Emanuel, 1994) but are also influenced by wind shear. This is apparent near the surface as seen in our companion paper Nilsson et al. (2015), which we will refer to as Part 1.

During the course of any day, the atmospheric boundary layer turbulence will naturally respond to different levels of shear and buoyancy production, directly influencing the level of turbulence kinetic energy (TKE). In addition, transport and dissipation of TKE can change substantially from hour-to-hour as well as on shorter and longer time scales, thereby influencing the level of TKE at specific heights in the ABL. Modeling the time evolution of the boundary layer for growth and decay phases of turbulence under unstable conditions can be a very challenging task, but it is important for many applications (e.g. dispersion of pollutants).

Several important earlier modeling studies of the daytime unstable ABL should be mentioned. The early work of Nieuwstadt and Brost (1986) and later studies of Pino et al. (2006) considered a very abrupt instantaneous shutdown of sensible heat flux to zero in large-eddy simulations (LES), which may best correspond to a modeling effort of unusual solar eclipse events. Sorbjan (1997) instead considered using a cosine shaped surface heat flux forcing, which can fit measurements relatively well for the afternoon time period (Nadeau et al., 2011). In Sorbjan (1997), a forcing time scale implying a length of the afternoon period of only about 1.4 h was used, which can often be considered very short in mid-latitudes. The study of van Driel and Jonker (2011) also performed idealized simulations for the unstable boundary layer using LES with

A simple TKE model

E. Nilsson et al.

|◄ | ►|

◄ | ►

Back | Close

Full Screen / Esc

Printer-friendly Version

Interactive Discussion

a variety of non-stationary surface heat flux forcing functions and emphasized that mixed-layer modeling can be quite successful as long as the forcing time scales are not short in comparison to the eddy turn-over time scale.

Goulart et al. (2003, 2010) studied TKE using a theoretical spectral model and LES data and showed a reduction in TKE decay during the afternoon transition when including wind shear in their modeling attempts. This was also clearly shown for TKE averaged over the boundary layer depth in Pino et al. (2006). Beare et al. (2006) also studied afternoon and evening transition leading up to the early morning boundary layer using LES and several studies (Brown et al., 2002; Kumar et al., 2006; Basu et al., 2008) also attempted to model a realistic diurnal cycle using large eddy simulation. These studies did not, however, specifically address the representation of the evolution of TKE. Rizza et al. (2013) did study TKE evolution with LES and showed that boundary layer averaged TKE can obtain exponents of the decay power law t^α from at least −2 to −6 as previously shown for surface layer TKE (Nadeau et al., 2011) using measurements.

For the Boundary Layer Late Afternoon and Sunset (BLLAST) field campaign, several LES studies (Blay-Carreras et al., 2013; Pietersen et al., 2014; Darbieu et al., 2015) have been carried out on specific days of the field campaign. These studies have provided analysis of TKE evolution and turbulence structure (Darbieu et al., 2015) and have taken into account of external forcing effects such as for instance subsidence (Pietersen et al., 2014; Blay-Carreras et al., 2013) and influence of the residual layer from a previous day on the growth of the morning boundary layer (Blay-Carreras et al., 2013). Model experiments for several days of the field campaign, rather than specific case studies, are also very beneficial for aiding in understanding the differences between days better. In the context of BLLAST, Couvreux et al. (2015) evaluate the ability of numerical weather prediction models to predict TKE evolution for all Intensive Observation Period (IOP) days. These studies did not, however, cover the evolution of the TKE budget in the afternoon transition.

Nadeau et al. (2011) managed to rather successfully model near-surface TKE decay in the afternoon for very convective days using a simple heuristic TKE budget model. Their model's only inputs are boundary layer depth and buoyancy flux, and uses a simple parametrization for dissipation of TKE. In Part 1, TKE budget calculations showed that a realistic modeling of near-surface TKE for the observational period during BLLAST requires accounting for shear production and vertical transport of TKE in addition to dissipation and buoyant production.

In this paper, we present a simple one-dimensional TKE budget model based on the analysis presented in Part 1 and assumptions about approximate height dependencies of TKE budget terms in the mixed-layer. We use this model to carry out simulations for nine IOP days where near-surface measurements and TKE budget estimates for both morning and afternoon periods were available. In this way, we can compare our simulated TKE at different heights to observations and discuss directly how the estimated budget terms act in the model to underestimate or overestimate TKE at specific times. We want to stress that this model has been developed with the aim of aiding in the understanding of the most important processes that govern TKE evolution for sheared convective situations, but it should not be regarded as a complete description of the complex reality. As will be discussed further in the text, the model does not include processes such as elevated shear production and horizontal advection of TKE, which may be important at specific times. We use observations from several different land cover-types to explore the sensitivity of the modeled boundary layer dissipation rates in relationship to those observed over the heterogeneous BLLAST field campaign landscape. This heterogeneity challenges some of our modeling assumptions. We insist on carrying out the study with a simple model for near-surface TKE and TKE budget terms because it is an important first step before more complexity and processes may be added. Compared to the model proposed in Nadeau et al. (2011), which required a prescribed boundary layer depth and near-surface buoyancy flux, we add a prescribed near-surface wind speed to carry out our modeling efforts.

The paper is structured as follows. In Sect. 2, we guide the reader to the relevant datasets used in the paper and further documentation about how the data were selected and treated for our modeling efforts. In Sect. 3, we describe the different parts of the simple TKE model and make a first comparison to data for the afternoon of 20 June 2011. This is followed in Sect. 4 by a further evaluation of near-surface TKE and TKE budget terms for nine simulated IOP days including discussion of potential sources of errors in TKE prediction. In Sect. 5, we explore modeled dissipation rate for the boundary layer, using observed fluxes and winds from different surface land covers and an area-averaged flux, in comparison to observed dissipation rate and discuss the formation of a "pre-residual layer" during the afternoon transition. In Sect. 6, we use the model to simulate near-surface TKE for a variety of idealized afternoon conditions and discuss the results in relationship to previously proposed "decay laws" of turbulence. Finally, we conclude and summarize in Sect. 7.

2 Data and methods

2.1 Description of data sets

Our proposed model is based on a simplified TKE budget including idealized height-varying terms for shear production, buoyant production, transport and dissipation. It is driven with surface measurements (wind speed and fluxes) and boundary layer depth z_i. In this section, we describe the observational dataset that is used (see Table 1) to drive the model, and to evaluate it on TKE budget term estimates.

Firstly, we will use wind speed and buoyancy flux from the Divergence site and z_i estimates from lidar measurements (all described in Part 1) to drive model simulations for 9 IOP days. The lidar measurements were chosen due to slightly less fluctuating estimates compared to the UHF (Ultra High Frequency) wind profiler estimates. On 26 June z_i from the UHF profiler was used because no lidar estimates were available. The hourly TKE budget results from the Divergence Site is also used to evaluate the

model TKE budget terms and near-surface TKE. Furthermore, TKE from the 60 m tower was computed at three measurement heights (29.3, 45.8 and 61.4 m) with the same procedure as described in Part 1. Hence, 10 min TKE values were calculated before any further 1 h running mean procedure was applied. For evaluation purposes also a limited set of data from a 3-D sonic anemometer suspended from a tethered balloon was used, see Lothon et al. (2014). For evaluation of boundary layer dissipation rate we also use estimates from a UHF wind profiler and measurements from full aircraft flight legs. These data sets are all found on the BLLAST database, see BLLAST (2015).

Secondly, as an exploration of the sensitivity in modeling results, we also use observed sensible and latent heat fluxes along with observed wind speed and temperature from 5 other land surface covers (moor, corn, grass, wheat and forest) to drive our TKE model. The fluxes are obtained from the uniformly processed data set by De Coster and Pietersen (2012) using the EC-PACK flux computation algorithm (Van Dijk et al., 2004). These flux time series are based on 30 min averaging periods and were also used by Hartogensis (2015) to derive area-averaged fluxes for the Plateau de Lannemezan area, based on the land use and complementary energy balance modeling for urban and bare-soil surfaces where no measurements were available. We will also show results for boundary layer dissipation rates based on such 2 by 2 km area-averaged fluxes centered on the 60 m tower in Sect 5. The specified data set including both observed time series, area-averaged fluxes, land use maps, documentation and quick-looks are found at the BLLAST website under the section "Area-averaged flux maps" in the BLLAST database.

In Table 1, we briefly summarize information about the surface datasets used. Here we also list the roughness length z_0 used in model simulations for the various sites. A value of 2 cm was estimated for the Divergence Site based on a period of reasonably steady winds in near neutral but slightly stable data (not morning or afternoon transition data). This value was also used for simplicity at all other sites and data sets except over the forest where it was increased by a factor of 10 and a displacement height of 2/3 of an estimated average tree height of 20 m was used (Garratt, 1992).

We will show results from 9 of the 10 IOP days previously considered in Part 1. This is because on 19 June there were no measurements available from the Divergence site before 10:00 UTC and we chose to consistently do simulations constrained by observations from the time of positive sensible heat flux in the morning until the end of the afternoon, defined from zero-buoyancy flux. This choice is to allow for the turbulence to build and decay during a long time period of sheared convective atmospheric conditions for each day.

2.2 Description of data time series treatment

The data sets described above all consist of estimates of different parameters, wind speed, buoyancy flux (or sensible and latent heat flux plus potential temperature that can be used to estimate buoyancy flux) and z_i at different temporal resolutions. Before using these data to drive our TKE model we formed time series of 1 s temporal resolution in the following manner.

The time from positive sensible heat flux until zero buoyancy flux was estimated for each day and time series manually checked. A few suspicious values in various times series were removed in this process. Then, a linear interpolation to 1 s values was applied followed by a 1 h running mean smoothing of the data. This procedure was adopted as we, especially for wind speed at these sites, found rapid variations in time and our intention is to attempt to model the more general slow decay of turbulence kinetic energy related to persistent changes in surface flux forcing and the slower trends observed in wind speed.

For boundary layer depth estimates, a 1 h running mean time series was formed in a similar way. Here, before linearly interpolating, a representative boundary layer depth value for the morning at the start of each simulation was subjectively estimated from the observed growing trend of z_i later in the morning. This was done despite of sometimes sparse observational estimates in the early morning. For the 9 considered days starting at 20 June and ending at 5 July the following 9 initial values of z_i was specified: (150, 250, 200, 150, 200, 150, 100, 200, 200) m. This was needed to have

a full time series of smoothly varying boundary layer depth evolution (i.e., $z_i(t)$) for the full time period of simulation, as required by the model (described below).

2.3 Treatment of dissipation rate from UHF wind profiler

For evaluation of our model the data set of UHF wind profiler data described in Part 1 also includes estimates of TKE dissipation rate. It was available at an average temporal resolution of 5 min and a spatial resolution of 75 m starting at a height of 175 m. We used the UHF profiler data from Site 1 (closest to the Divergence Site tower and 60 m tower, Lothon et al., 2014). These estimates of dissipation rate were based on Doppler spectral width following Jacoby-Koaly et al. (2002). Best estimates were formed from the median of the four oblique beams. We used the same software as described in Part 1 from Garcia (2010) to gap-fill and smooth the data set. The data were placed on a uniform time-height grid by observational minute and using the 75 m vertical resolution. Then, a smoothing parameter S of 10^{-1} was used with 5 repeated iterations and an extra smoothing in time using a 15 min running mean value for each vertical level.

For evaluation, we also compared model estimates with UHF estimates and aircraft estimates of TKE dissipation rate from the Piper Aztec research airplane (Lothon et al., 2014). For that comparison, a further averaging of the UHF data for the same observational times as the corresponding flight legs followed by interpolation to the average height of the flight leg was performed.

To display the slower trends and evolution of TKE dissipation rate in a height time representation, the 5 or 15 min averaged datasets was considered still quite scattered and a running mean value of one hour was applied for comparison with the modeled dissipation rate. This is reasonable here because we use a 1 h smoothed wind and surface flux time series as input to force the model and hence do not model the more temporary rapid variations of TKE budget terms.

3   Model description and evaluation for the afternoon of 20 June 2011

In this section, we describe a simple model for the atmospheric boundary and surface layer turbulence kinetic energy and make a first comparison between model results and observations for the afternoon period of 20 June.

3.1   The governing TKE equation

In this work, we consider a simplified budget for TKE of the following form, assuming no advection and horizontal homogeneity:

$$\underbrace{\frac{\partial E}{\partial t}}_{\text{Tendency}} = \underbrace{-\overline{u'w'}\frac{\partial U}{\partial z}}_{\text{Shear production:}S} + \underbrace{\frac{g}{\overline{\theta}}\overline{w'\theta'_v}}_{\text{Buoyancy production:}B} \underbrace{-\frac{\partial \overline{w'E'}}{\partial z} - \frac{\partial \overline{w'p'/\rho_0}}{\partial z}}_{\text{Transport:}T} \underbrace{-\epsilon}_{\text{Dissipation:}D}. \tag{1}$$

Here, TKE $(= E)$ denotes $\frac{1}{2}\left(\overline{u'^2} + \overline{v'^2} + \overline{w'^2}\right)$, where u', v' and w' are respectively the instantaneous deviations of along-wind, cross-wind, and vertical wind components from their respective mean values. U is the magnitude of the mean wind, which varies with height, z; g is the acceleration of gravity; $\overline{\theta}$ is mean absolute temperature; θ'_v is the instantaneous deviation of virtual potential temperature from its mean value; ρ_0 is the air density; p' is the instantaneous deviation of air pressure; and ϵ is the mean dissipation rate of TKE.

The physical interpretation of the five terms in Eq. (1) from left to right is: local time rate of change of TKE; shear production of TKE; buoyancy production of TKE; vertical divergence of the total transport of TKE; and dissipation rate of TKE.

Given simple parametrization for the right hand side terms of Eq. (1) and specified initial profile of the TKE, the budget equation can be used to solve for the evolution of turbulence kinetic energy $E(t)$. Below we describe the simple modeling of surface fluxes, the assumed flux gradient relationship, treatment of the height dependence of the various budget terms and the initial conditions.

3.2 Treatment of surface fluxes, flux gradient relationship

An important driving force for the atmospheric boundary layer turbulence in unstable conditions is the surface buoyancy flux, which controls near surface buoyancy production in this simple model. In first instance, we will prescribe these, as determined in Part 1, from the 3.23 m level of the Divergence Site. In Sect. 5, we will go on to use the preprocessed available time series of sensible heat flux (SH), latent heat flux ($L_v E$) and observed potential temperature time series $\overline{\theta}$ from the other surfaces. The following relationship is then used assuming there is no influence from liquid water flux:

$$B_0 = \frac{g}{\rho c_p \overline{\theta}} \left(\text{SH} + (0.61 c_p \overline{\theta} / L_v) L_v E \right). \tag{2}$$

Here, B_0 is the buoyancy production term used at the first grid point above the surface (or above the displacement height d in the case of the forest), c_p is the specific heat capacity of air, and L_v is the specific latent heat of vaporization.

In Part 1, shear production was shown to be an important source of turbulence production, especially near the surface. To model shear production, we use an idealized Monin–Obukhov similarity-based flux gradient relationship (Wilson, 2001) to determine the vertical gradient of mean wind speed strictly applicable to a locally homogeneous quasi-steady atmospheric surface layer:

$$\frac{\partial U}{\partial z} = \frac{u_*}{kz} \phi_{\mathrm{m}} \left(\frac{z}{L} \right). \tag{3}$$

Here, u_* is friction velocity, k the von Karman constant (set to 0.4) and L is the Obukhov length scale ($L = -\frac{\overline{\theta} u_*^3}{kg(\overline{w'\theta_v'})_0}$), in which $(\overline{w'\theta_v'})_0$ is the kinematic virtual temperature flux at surface. Based on fits to extensive data from Högström (1988), Wilson (2001) proposed the following functional form for the non-dimensional wind gradient, ϕ_{m}:

$$\phi_{\mathrm{m}} = \left(1 + 3.6|z/L|^{2/3} \right)^{-1/2}, \tag{4}$$

which for unstable conditions integrates to the relatively simple mean wind profile

$$U(z) = \frac{u_*}{k}\left[\ln\frac{z}{z_0} - 3\ln\left(\frac{1 + \sqrt{1 + 3.6|z/L|^{2/3}}}{1 + \sqrt{1 + 3.6|z_0/L|^{2/3}}}\right)\right].$$ (5)

It should be noted here that a different functional form for the non-dimensional wind gradient was found in Part 1, but here we chose to keep the consensus value of von Karmans constant. We consider it may be other non-dimensional parameters than z/L that is also needed to improve shear production estimates. As we shall see in Sect. 4 the chosen functional form provides a reasonable wind gradient and shear production very near the surface, but less good at increasing height.

To use the above wind speed relationship, we need to determine a u_* value which also enters into the Obukhov length L. To do this, the wind speed is first extrapolated from the measurement height z_m to $z = 10$ m using

$$U_{10} = U_m\frac{\ln(10/z_0)}{\ln(z_m/z_0)}.$$ (6)

A simple drag coefficient or CD-curve approach (CD = u_*^2/U_{10}^2) is then used to form an initial estimate of u_* with the following relationship (determined from measurements, see Fig. 1):

$$CD = A_{CD}U_{10} + B_{CD},$$ (7)

where the empirical coefficients were computed to be $A_{CD} = 2 \times 10^{-3}$ s m^{-1} and $B_{CD} = 5 \times 10^{-3}$ (unitless).

Using such a u_* value directly in Eq. (5) would, however, not produce a wind speed that is consistent with the measured mean wind speed at height z_m. Therefore, an iterative approach is used to determine a stability corrected u_* value in the following

way. Firstly, a value for Obukhov length is calculated. Then, Eq. (5) is rewritten to solve for u_* taking into account the influence of stability:

$$u_* = (kU(z_m)) / \left[\ln \frac{z_m}{z_0} - 3 \ln \left(\frac{1 + \sqrt{1 + 3.6|z_m/L|^{2/3}}}{1 + \sqrt{1 + 3.6|z_0/L|^{2/3}}} \right) \right] \tag{8}$$

This new u_* value is used to calculate a new Obukhov length and the process is repeated ten times so that converged u_* and L values are reached. Usually only two or three iterations are needed for sufficient convergence.

In Fig. 1, the measured and modeled u_* values are plotted as a function of wind speed. Some variability is missed with this approach and it may lead to systematic underestimation in the modeled u_* when winds are higher than $2\,\mathrm{m\,s^{-1}}$. As will be evident from time series presented in Section 4, some of the high values of measured u_* at 3.23 m are, however, occurring very temporarily and are not always clearly linked to the mean wind at 8 or 10 m. Hence, they are likely not being well-predicted by the relationship formed from the input of one mean wind at one height.

3.3 Height variation of modeled TKE budget terms

Here, we describe the vertical height dependence that is assumed for each of the right hand side budget terms of Eq. (1). At the same time, we will discuss the behavior of the corresponding measurements from the Divergence Site tower at four times during the afternoon of 20 June.

3.3.1 Height dependence of the buoyancy term

To describe the height variation in the boundary layer, we use idealized linear profiles of buoyant production for a quasi-steady, horizontally homogeneous boundary layer following Lenschow et al. (1980). We set an entrainment parameter B_E to −0.15 by

analysis of the large-eddy simulation results for 20 June from Darbieu et al. (2015). In Fig. 2, the normalized profile of buoyant production in the model is shown in the far left panel. A linear decay is also assumed from z_i up to a height of no turbulence z_{i0}, which is defined from the vertical transport of TKE in Sect. 3.3.3. In comparison to proposed modeling of this TKE budget term in Lenschow (1974) the main difference is a further inclusion of some more fitting parameters for the shape of the vertical profile in the normalized height interval $0.87 \leq z/z_i \leq 1$ in their case (see Eq. A3 in Appendix A). Also, they make no prediction of TKE budget terms above the boundary layer depth.

In the middle and right panels of Fig. 2, we show the profiles of modeled buoyant production at four times during the afternoon transition. Near-surface hourly budget estimates centered on the corresponding times are also included. Boundary layer depth z_i is prescribed from observed smoothed lidar measurements and hence evolve in time, but for clarity only z_i and z_{i0} at 12:30 UTC are included as black and light blue horizontal lines. It is clear that at 12:30 and 14:30 UTC the two upper measurement levels show higher values of buoyant production than the model. It is possible that some influence of large-scale sub-meso or meso-scale fluctuations are causing higher values of fluxes at these heights in convective conditions. It is, however, unclear if such features should be considered turbulence. We ignore some of these higher values, which is, as will be shown later, also not as consistent in time as the 3.23 m level measurements. It is, however, important to remember when interpreting these results that transport is calculated as a residual from other budget terms as described in Part 1.

3.3.2 Height dependence of the shear production term

The shear production considered in this simple model is given by $-\overline{u'w'}(z)\frac{\partial U}{\partial z}$, where the wind gradient is given by the expression discussed in Sect. 3.2. For the profile of stress, we first form a surface value $\overline{u'w'}_0 = -u_*^2$ and then a linear decay of the stress profile with height is assumed. More specifically, we assume that it decays to a value of 0 at z_{i0}, where there is no turbulence and hence no stresses. Assuming linear stress profiles may be very reasonable for very convective conditions (Deardorff,

1972; Wyngaard, 2010) when their curvature is decreased to nearly zero and the contribution of $\overline{v'w'}$ stresses may also be smaller (Wyngaard, 2010). In more neutral conditions these assumptions may be more questionable, but keeping with our aim to formulate a simple model, we keep the assumption of linear stress profiles for all stability conditions. Also, Verkaik and Holtslag (2007) observed nearly linearly decaying momentum flux in slightly unstable conditions from several wind sectors and increasing momentum flux divergence with increasing stability in data from the Cabauw tower in the Netherlands. Lenschow (1974) explored both assuming a constant shearing stress (their model with this assumption is repeated in Appendix A) or a linearly decaying shear stress in the mixed layer. Lenschow (1974) also used a slightly different normalized wind gradient than us, but in general very similar results were obtained. We multiply our stress profile with the wind gradient expression (given by Eq. 3) to calculate the shear production term S at each height. Very close to the surface, any shear production term that involves a logarithmic wind dependence will form a very high value. To address this, we replaced our first grid point value at 1 m above the surface (or first grid point above displacement height in the forest case) with a linear extrapolation of the second and third model level values.

In Fig. 3, we show the modeled and observed shear production for the afternoon of 20 June. It is clear that even though the model has roughly the correct order of magnitude at 2.23 and 3.23 m, the modeled shear production term is decaying too quickly with height to a value of near zero at about 60 m. The measured shear production may instead indicate that in the middle of the boundary layer, some mixed layer shear production takes place, which is not accounted for in this model driven by only surface measurements and boundary layer depth z_i. The wind gradient expression we have used is also only meant to be used in the surface layer, and our measurements may suggest that it works best only in the limit of low heights.

3.3.3 Height dependence of transport of TKE

Figure 4 shows the modeled and observed transport term of the TKE budget. The modeled transport term consists of both a transport due to buoyancy produced TKE and shear produced TKE. Such an approach may of course be criticized as turbulence in reality cannot be separated in such a way, but we are nevertheless not the first (Mangia et al., 2000) to suggest such an approach when attempting to simplify the situation for a simple model. Based on studying vertical profiles of transport in sheared convective large-eddy simulations, we adapt a very idealized transport term T which consists in one part T_b more directly related to the buoyant production and one transport T_s that is related to the shear production term. At each height they are related as:

$$T = T_b + T_s. \tag{9}$$

The term T_b is given by a linear increase with height with slope k_1 for heights z up to the boundary layer depth z_i as:

$$T_b(z) = T_{b_0} + k_1 z. \tag{10}$$

At the boundary layer height z_i, the term reaches a maximum value $T_{b_{max}}$ and above the boundary layer depth a symmetric $-k_1$ slope is assumed so that the T_b is given by:

$$T_b(z) = T_{b_{max}} - k_1(z - z_i). \tag{11}$$

This also determines the height of no turbulence z_{i0} as the height above z_i where $T_b(z)$ becomes 0. The surface value T_{b_0} needs to be specified and it is determined by a fraction T_f of the total transport to the total near surface production and the time dependent surface buoyant production of TKE as

$$T_{b_0}(t) = -T_f B_0(t). \tag{12}$$

We shall soon determine T_f from measurements, but first to solve Eqs. (10) and (11) we also need the slope k_1 which is given by:

$$k_1 = \frac{T_{b_{max}} - T_{b_0}}{z_i - 0}. \tag{13}$$

We solve for $T_{b_{max}}$ by requiring that the transport term T_b integrates to zero over the depth of the turbulent boundary layer. That is, from the surface to z_{i0}. Given the transport fraction T_f, the term T_b can now be solved for, but this only makes up one part of the total transport term in the model. In accordance with Eq. (9), we will first describe the transport related to shear production T_s. This term is given by the expression:

$$T_s(z,t) = -(T_f - p)S(z,t)(1 - z/z_{i0}). \tag{14}$$

$S(z,t)$ is the height and time dependent shear production, T_f is the near surface transport fraction and p is a small positive free parameter that is determined such that the transport term T_s integrates to zero over the depth of the turbulent boundary layer. This produces a transport profile with a negative layer near the surface transporting some of the near-surface shear generated TKE to the upper levels and a positive area above, that spreads the transport over the turbulent boundary layer. It also implies that the factor p alters the near surface transport fraction value, but usually only a few percent.

Finally, the transport fraction T_f, defined as the ratio of (minus) the total near surface transport and the sum of near surface shear and buoyancy production, is given as a z/L dependent function, based on our TKE budget analysis in Part 1 where we determined ϕ_T, ϕ_b and ϕ_m, such that:

$$T_f(z/L) = \frac{-\phi_T}{\phi_b + \phi_m} = 1 + \frac{0.54z/L - 0.45}{0.7(1 - 15z/L)^{-1/4} - z/L}. \tag{15}$$

Equation (15) is compared to measurements in unstable conditions in Fig. 5, both for the afternoon and morning period with 4 orders of magnitude of variation in terms

of the stability parameter z/L. It is a good match to data for the morning period (blue circles and bin-averaged data with error bars) except possibly very close to neutral where the error bars are much larger mainly because of a specific time period in the morning of 25 June with indication of transport to the near-surface layers either from above or through a horizontal advection of TKE. Also, in comparison to the afternoon data, the expression is a good match very near neutral, but it potentially overestimates transport over the range of $-z/L$ between about 0.5 to 7. It is, however, within the one standard deviation error bars. A different z/L expression, which may fit the afternoon data better, would still not be general as it would degrade the performance during the morning period. Future work should be aimed at understanding if the observed difference between the build-up and the decay phases of turbulence are linked to some other non-dimensional parameter combination. As a first approximation, we apply the presented relationship at the first grid point 1 m above the surface in our model. In the case of the forest, the relationship is instead applied at the first grid point above displacement height d.

The resulting profile of total transport shown in Fig.4 compare qualitatively quite well to the modeled transport term in Lenschow (1974) with a negative layer in the lower boundary layer and positive layer above. A linear profile shape in the mixed layer and a stronger curvature near the surface due to the effect of shear production is also present in both models (Figs. A1 and A2). The exact value of this term on specific heights differ, however, between these two models due to our inclusion of TKE budget terms also above the boundary layer depth z_i and because of our specified near-surface transport fraction. In near-neutral conditions the model from Lenschow (1974) obtain negligible transport in comparison to shear production and dissipation terms (see Fig. A2) whereas we retain more transport also in these conditions (with $T_f \approx 0.36$). For very convective conditions we obtained $T_f = 0.46$ whereas Lenschow (1974) has a transport fraction $T_f \approx 0.57$. This is of course an uncertain parameter that could be investigated more in future work. Data from Dupuis et al. (1997) may for instance suggest a value as large as 0.69 in convective conditions.

3.3.4 Height dependence of the dissipation term

The dissipation rate of TKE is calculated in the model using the TKE length scale parametrization presented in Part 1:

$$D = -\frac{E^{3/2}}{l_\varepsilon} = -E^{3/2}\left(\frac{2.2}{z_i} + \frac{0.006}{z}\right).$$ (16)

The modeled profiles of dissipation for the afternoon of 20 June are shown in Fig. 6 as colored lines and shown with both the near-surface dissipation as dots, UHF wind profiler estimates from 175 m as lines with circles and estimates from aircraft as crosses at two height intervals of 75 m for 14:30 and 17:30 UTC. Near the surface, it is clear that the modeled dissipation decays more rapidly with height than it should because of too rapidly decaying in the shear production term, leaving to little shear produced TKE ($= E$) at 8 m. The modeled dissipation in the boundary layer compares well to the aircraft estimates of dissipation and in order of magnitude to the UHF profiler estimates. However, the UHF profiler estimates shows a maximum at some height around 500–600 m, which the model and aircraft measurements do not show. It is not easily determined if this often seen feature in UHF profiler estimates is realistic. Large-eddy simulations for this day did not show a pronounced maxima in dissipation rate. The only way our simple parametrization could produce such a maxima in dissipation rate is if the TKE itself has a maximum at these heights. Vertical wind variance is well known to have a maximum at some height around 0.3–0.4z_i, whereas LES often produce a maximum of TKE closer to the surface (below 100 m). Also, this simple model predicts such a feature on several of the more convective days at around 40–50 m but fails to do so on 20 June as we will see in the next subsection. Qualitatively the vertical profile of dissipation is similar in our model compared to the model from Lenschow (1974), illustrated in Figs. A1 and A2, with higher dissipation closer to the ground but with some important differences with increasing height. The dissipation approaches a constant value with height in the model from Lenschow (1974) whereas in our case

it responds to the decreasing turbulence levels with increasing height. The exact level of dissipation in the two models close to the surface is also different under different stratification, mainly due to our different approaches to model vertical transport of TKE.

3.3.5 Height and time dependence of TKE

The evolution of TKE is determined by a finite difference (forward in time) calculation with 1 s time step and 1 m vertical resolution from the other budget terms using the TKE budget equation.

$$\frac{E(z, t_{n+1}) - E(z, t_n)}{\Delta t} = S(z, t_n) + B(z, t_n) + T(z, t_n) + D(z, t_n) \tag{17}$$

The resulting vertical profiles of TKE are shown in Fig. 7 for the afternoon of 20 June. In this figure, TKE at the small tower (2.23–8.22 m) was averaged and a standard deviation was calculated for each hour centered around 12:30, 14:30, 16:30 and 17:30 UTC. The result is shown with a vertical error bar indicating the minimum and maximum of the data. The same procedure was applied for the 60 m tower data, which consistently showed lower TKE levels compared to the near surface TKE. The procedure was also applied to limited 3-D-sonic anemometer data from a sensor suspended from a tethered balloon (see Lothon et al., 2014, for details). Data were available at ≈ 70 m and 520 m above ground at 12:30 and 17:30 UTC. At 14:30 and 16:30 UTC, the tower data has been slightly vertically displaced to better show the error bars without overlapping too much.

It is clear that the model produces TKE of the right order of magnitude and predicts the general reduction of TKE with height from the smaller tower to the 60 m tower. The decay of TKE in time may, however, be somewhat to rapid in comparison to measurements, as indicated by the low TKE levels at 16:30 and 17:30 UTC. However, the individual levels on the towers (2.23 and 61.4 m) will be shown in time series plots in the next section which have quite reasonable levels of TKE for 20 June considering the large variability in 10 min values that occurs during these convective conditions.

A simple TKE model

E. Nilsson et al.

Title Page

Abstract | Introduction

Conclusions | References

Tables | Figures

|◄ | ►|

◄ | ►

Back | Close

Full Screen / Esc

Printer-friendly Version

Interactive Discussion

The model only predicts an increase of TKE from the first model level to the second, due to the prescribed reduced shear production at the first grid point compared to the others. Otherwise, the model shows a decrease in TKE with height, which is not necessarily true at all height ranges. The measurements often show a small increase in TKE from 2.23 to 8.22 m (as is clear from Table B3 in Part 1), but consistently lower TKE levels at the 60 m tower imply a maximum of TKE somewhere close to the surface at a height on the order of tens of meters. As mentioned above, this simple model is capable of predicting a maximum of TKE near the surface at around 40–50 m for some of the more convective days of the field campaign. Then the model also often overestimates the TKE level at the 60 m tower. This could indicate that the maximum of TKE should be placed even lower than 40 m.

3.3.6 Specification of initial neutral morning conditions

The TKE budget equation is used to solve for the evolution of TKE from neutral morning conditions until the end of the afternoon. At the beginning of the simulation, for simplicity, we therefore assume the buoyant production term $B(z)$ to be zero at all heights. The shear production term $S(z)$ is calculated as before. The transport term is in this case only specified from the transport fraction and the shear term as $-S(z)T_f$ to avoid an uncompensated positive layer in the upper part of the boundary layer.

Our treatment of initial conditions for dissipation $D(z)$ and turbulence kinetic energy $E(z)$ also differs from other time steps since there is no history of the flow to take into consideration at the first time step. Here, we first assume that the initial TKE tendency is negligible (such that $\frac{\partial E}{\partial t} = 0$) and then solve for $D(z)$ based on the shear production and transport term, hence $D(z) = -(S(z) + T(z))$. Then, we use this initial dissipation and estimate an initial TKE profile from $E(z) = \left(\frac{-z_i D(z)}{2} \right)^{2/3}$ such that the dissipation in the following time step will not obtain a large sudden jump when using the profile $E(z)$ to estimate dissipation using Eq. (16). It should be mentioned that height z (or height above the displacement height in case of the forest) is for simplicity ignored here, but

model tests showed small differences in results for the evolution of modeled TKE at midday and afternoon.

4   Evaluation of near surface TKE and budget terms: 9 IOP days

In this section, we compare the simple model to measurements for 9 IOP days studied in Part 1. The first objective is to investigate the simple model's ability to predict a reasonable near surface TKE and TKE budget evolution for the diverse set of conditions that occurred on these 9 days despite its deficiencies. The second aim is to discuss why the model produces unreasonable results. This indicates potential focus areas for future model improvement.

The upper row of Fig. 8 shows the model's stability corrected friction velocity u_* as black lines and observations at 3.23 m as red lines with dots. It is clear that our approach gives reasonable estimates of u_* on many occasions, but also it misses some low and especially high values that occur for periods of 1 or 2 h. Further, the modeled friction velocity, based on mainly the mean wind speed, does not always reflect this observed variability and produces a more smooth evolution of u_* for each day.

The middle row of Fig. 8 shows the measured wind speed gradient based on 10 min values as thin colored lines with dots and the modeled wind speed gradient as thicker colored lines. In this case, it is clear that wind gradients shift rapidly and the model captures some of the low frequency variability of the observations. This is, however, not always the case (see e.g., 27 June as well as 2 and 5 July).

The observed hourly shear production is shown in the lower row of Fig. 8 with colored dots. The model (thick lines) does capture some of the day to day variability, but the smooth model results do not capture all of the individual hourly variability seen in the measurements. Furthermore, shear production tends to be underestimated at times with higher shear production such as on 25 and 26 June. This underestimation is more severe at 8 m as a consequence of the shear production height dependence, which decays too rapidly with height. This is seen on 25 and 26 June, at the end of the

afternoon of 27 June and to some extent, on 20 June and in the middle of the day on 1 July.

The observed and modeled near surface buoyant production is shown in the upper row of Fig. 9 and is in general a good (albeit smoothed) representation of the measurements. On 20 June at 12:30 UTC, the model underestimates the measured buoyancy production at 5.27 and 8.22 m as was already noted in Fig. 3. On 30 June, which had variable cloud cover, similar errors are also seen, but otherwise in most cases the differences between model and measurements are smaller for this more directly forced budget term.

The middle row of Fig. 9 shows the modeled and observed transport, which show significantly larger scatter in observed values compared to the buoyant production and larger individual discrepancies between model and measurements. Particularly on days with more wind, the scatter is larger such as on 20, 25–27 June. As discussed, it is challenging for the model to capture the shear production well on an hourly basis and also the modeled transport has a smoother evolution in time than the observations.

The lower row shows the observed and modeled dissipation. The model captures much of the day to day as well as hourly variability, but at times of strong shear production, it underestimates at the 8.22 m level. This is observed on 25, 26 and the afternoon of 27 June as well as in the middle of the day on 1 July. The model also overestimates dissipation somewhat on 2 July and during the morning period of 5 July until around 12:00 UTC.

All these observed errors in the modeled TKE budget terms, which may at times be considered quite small, can lead to problems in the prediction of the TKE as any systematic errors can cause an accumulated effect for the TKE prediction. We therefore find the modeled results of TKE at the 2.23 m level and 61.4 m level presented in Fig. 10 quite encouraging and indicative that our reported budget term expressions can reproduce well the overall level of observed TKE. There are, however, obvious discrepancies between the model and measurements that need to be discussed further.

For the 2.23 m level, shown in the lower row of Fig. 10, the model underestimates the TKE on 8 out of 10 days at the beginning of the simulation up until around 08:00 or 09:00 UTC (at least). This is probably mostly related to uncertainty in the way we define initial profiles of TKE for neutral morning conditions. The level of TKE at 2 m during midday is relatively well-captured on many of the days but too low on 2 and 5 July. On 2 July and the morning of 5 July this could be due to a slight overestimation of near surface dissipation. On 5 July there are also a few hours of an observed positive transport term at some heights (and small at other heights), implying a potential import of near surface TKE, which if it did occur cannot be captured by the simple model. This was also observed very temporarily on 27 and 30 June, which as discussed in Part 1, could be related to variable cloud cover and/or uncertainty in dissipation estimates. With this one dimensional model, it is difficult to draw conclusions regarding the import of TKE from above or by horizontal advection. On the morning of 25 June, however, there are several hours with observed positive values of the transport term at all measurement heights and this may have additionally contributed to an underestimation of near surface TKE in the morning of this day.

At 61.4 m, the TKE level is underestimated on 25 and 26 June and at the end of the afternoon on 27 June. It is likely a consequence of too rapidly decaying shear production with height. The model also tends to overestimate TKE on some days with higher buoyancy production (e.g. 24, 30 June, 1 and 2 July). It is unclear, however, to what extent the observed differences at 60 m should be related to issues with the model or related to differences in fluxes and wind that occur at different surfaces in the landscape surrounding the 60 m tower. It may of course be that the observed flux and wind at the Divergence Site is not always representative for a height of 60 m. A flux footprint analysis (Hartogensis, 2015) for the 60 m tower indicates that grass and moor (with relatively low fluxes similar to those observed at the Divergence Site) dominate the fluxes in unstable conditions at the 60 m tower, usually accounting for about 65 to 85 % of a reconstructed flux. With the remaining reconstructed flux related mainly to forest, urban and bare soil land surfaces. When the wind comes from the North or

North-East the flux is especially dominated by grass and moor conditions (Hartogensis, 2015), but this changes when the wind comes from East. Interestingly we observe that the model underestimates the TKE especially when the wind in the lower CBL and near the surface is from East, rather than typically from North or North-East for the rest of the time. The easterly flows happen on 25 and 26 June, in the late afternoon of 27 June and in the morning of 5 July (see wind direction close to the surface in Part 1, Fig. 3). All these periods correspond to an underestimated TKE in the model at 61.4 m. This could be linked with the presence of a band of forest to the East and the Lannemezan village behind, and that either the flux or the shear production that we use do not represent their effect. It could also be due to advected TKE from the East. These effects related to heterogeneity in the landscape in combination with shifting wind direction also causes the reconstructed flux (at the 60 m tower) to have a variable contribution from different surface land covers both on a daily and hourly basis. A flux footprint analysis may, however, not be directly translated to apply for a variable such as TKE. Therefore we mainly conclude that the model performs reasonably well at 2.23 m and less well, but still with the right order of magnitude for TKE at 61.4 m.

5 Sensitivity test of surface boundary conditions: influence on boundary layer dissipation rate and the formation of a pre-residual layer

As an exploration into the sensitivity of model results to different observed fluxes and winds over different surface types, we show in Fig. 11 modeled dissipation rate for 30 June from five simulations over corn, moor, forest, wheat and grass with available measurements. Also shown are model results for the Divergence site and using a 2 by 2 km area-averaged flux, as well as the observed dissipation rate from a UHF wind profiler. On this day, there was no distinguishable bias between dissipation rates from the UHF profiler and aircraft measurements (not shown here) and therefore a comparison of the overall modeled boundary layer dissipation with the observations from the UHF profiler is reasonable to make.

The Divergence Site tower measurements show very similar low fluxes as observed over grass and moor, and for this day, also corn. This is in contrast to the higher observed fluxes over forest and wheat. The surface flux over the grass, moor, corn and Divergence sites yielded the most similar levels of dissipation rate compared to the observations on this day, whereas other surface types lead to higher levels of dissipation rate. Based on energy balance modeling, fluxes of urban and bare soil land covers were also determined to be high, corresponding roughly to the forest level (Hartogensis, 2015). Especially, we believe that the urban land cover used likely overestimate the real flux from the villages considered here, which have much vegetation between the houses. Therefore, using area averaged fluxes over a $2\,\mathrm{km} \times 2\,\mathrm{km}$ or $10\,\mathrm{km} \times 10\,\mathrm{km}$ area of the surroundings lead to higher estimates of boundary layer TKE and dissipation rates compared to using the Divergence Site observations.

We note that the model may overestimate boundary layer dissipation somewhat for 30 June and turbulence may not be as capped in the model as indicated from UHF profiler. The simple model presented here lacks elevated wind shear in the entrainment zone, which may lead to an underestimation of dissipation rate and TKE in the upper parts of the boundary layer. Elevated shear may, however, also affect the entrainment process and the entrainment parameter which here has been simply taken as a constant value of -0.15 based on a study for 20 June. Model tests changing this value to -0.3 showed reduced levels of TKE and dissipation rate in the upper parts of the boundary layer, but with otherwise similar results and only a small impact in the lower part of the boundary layer.

An apparently important result from this study is that the modeled decay of dissipation rate and TKE occurs first at the upper part of the boundary layer during the afternoon as a response to the diminishing surface buoyancy flux forcing. This may, of course, in reality be prevented by the presence of elevated wind shear, but on most of the days it is also observed by the UHF profiler. Grimsdell and Angevine (2002) and Lothon et al. (2014) also revealed, with remote sensing observations, a decay

of TKE dissipation rates from top to bottom (although not systematically). This was also used as a way to define a top of the turbulent boundary layer in the afternoon transition in numerical weather prediction models (Couvreux et al., 2015). In Fig. 11 the white line shown is an iso-line for TKE (corresponding to $0.3\,\mathrm{m^2\,s^{-2}}$), which is of course an arbitrarily chosen value, but it indicates low turbulence levels. It is instructive from a conceptual point of view to consider these conditions with low turbulence levels during the afternoon transition as a pre-residual layer. It forms when the boundary layer turbulence adjusts to the weaker buoyancy flux forcing from the surface. It is capped by the mixed-layer inversion and does not reach the surface except possibly very near neutral stratification at the end of the afternoon or the beginning of the evening transition. It is useful to introduce this concept of a pre-residual layer as we consider that it is an important part of explaining the onset turbulence conditions for the nocturnal residual layer.

The residual layer is defined as the statically neutral layer, characterized by weak sporadic turbulence, that lies above the stable boundary layer and below the capping inversion, separating the boundary layer flow from the free atmosphere. By definition, it begins to develop only after the surface begins to stably stratify. Therefore, it is useful to also name the region of weak turbulence that exists during unstable conditions preceding the residual layer as the pre-residual layer. It is within these continuously weakening afternoon turbulence conditions that many things characterizing the turbulence are changing, such as the shape of spectra of vertical wind velocity and integral length scales (Darbieu et al., 2015). Darbieu et al. (2015) showed with LES and measurements that change occurs first in the upper part of the boundary layer during the later stages of the afternoon transition, and the higher within the ABL the stronger the spectra changes. These observations may hence be considered to have taken place in the pre-residual layer and may potentially provide other ways to define and characterize it more exhaustively in the future.

6 Parameter exploration for near-surface TKE

In this section, we first discuss modeled near-surface TKE for the afternoon based upon complementary idealized numerical simulations. Secondly, we compare our numerical model results to a simplified analytical expression assuming quasi-stationary turbulence. Finally, we illustrate and discuss the added value of our modeling efforts taking into account variations in wind or u_* compared to only taking into account of w_* as a scaling variable for TKE.

The sensible heat flux used in these model runs are provided by a cosine function as in Sorbjan (1997) and several other earlier studies:

$$H_{\cos}(t') = H_{\max} \cos\left(\frac{2t'}{\pi\tau_{\cos}}\right). \tag{18}$$

Here, $H_{\max}$ defines the maximum sensible heat flux in midday and the decay time scale $\tau_{\cos}$ defines the length of the period with positive sensible heat flux (half of which covers the afternoon period). For simplicity, we chose a zero latent heat flux in these idealized simulations.

For boundary layer depth, we specify a very simple sine function increase of z_i from a neutral morning value $z_{i_{\min}}$ to a midday value $z_{i_{\max}}$ by

$$z_i(t') = z_{i_{\min}} + (z_{i_{\max}} - z_{i_{\min}}) \sin\left(\frac{2t'}{\pi\tau_{\cos}}\right), \tag{19}$$

which is then kept constant for the afternoon.

The complementary idealized numerical simulations have been performed by systematically varying a studied parameter while keeping all the other variables specified according to a reference simulation. We begin by providing the details of the reference simulation. For this simulation, we keep the wind speed constant at $2\,\mathrm{m\,s^{-1}}$ throughout the whole simulation. However, this does not mean a constant u_* value in the case of unstable stratification because of the stability correction of u_* and

flux gradient relationship described in Sect. 3.2. A mean temperature of 20 °C with a corresponding density of air $\rho = 1.205\,\mathrm{kg\,m^{-3}}$ and specific heat capacity is used, as well as a roughness length $z_0 = 0.02\,\mathrm{m}$ and entrainment parameter $B_E = -0.15$. The morning boundary layer depth $z_{i_{\min}}$ was kept at 150 m in all simulations. The values of the specific parameter settings which we vary for the reference simulation are given in Table 2 column 3.

We conduct six different types of model experiment test runs denoted by: AL (afternoon length), BLD (boundary layer depth), SH (sensible heat flux), U_c (constant mean wind speed), U_{inc} (Increasing wind speed), and U_{dec} (decreasing wind speed) runs. For each of these one variable of interest is changed. For the AL, BLD and SH, it is simply the variables $\tau_{\cos}$, $z_{i_{\max}}$ and $H_{\max}$ that is systematically varied. For the U_{mean} runs, it is a specified constant wind speed throughout the entire simulation that is varied. For the U_{inc} runs, we instead keep the wind speed at zero until midday and then increase it linearly to a specified value U_1 at the end of the afternoon (that is a normalized time of 1 after dividing with the afternoon length). In this way we study one of the simplest cases of a time-varying wind speed for the afternoon. Similarly, in the U_{dec} runs we instead let the wind speed be constant for the morning period until mid-day at a value denoted U_0 and then specify a linear decrease of wind speed to a value of zero at the end of the afternoon. In columns 4 and 5 of Table 2 and continued in Table 3, we list the parameter settings for our model experiment test runs. For shortening of the table, we denote our U_1 and U_0 settings by U_{c^*}, which means the same numerical values from 0 to $3\,\mathrm{m\,s^{-1}}$ were used as in our constant mean wind speed runs U_c. It should be noted that these settings represent a range of conditions encountered during the BLLAST field experiment.

Here, only 2 m results from our idealized modeling will be discussed since the model compares well with measurements of TKE at 2.23 m in the previous section and less well at other heights. Our AL runs indicated that varying the afternoon length played a small role on the near-surface TKE results (not shown here). After normalization with the afternoon length, the results collapsed to within 1–2 % of each other with a slight

tendency that longer afternoon lengths resulted in lower TKE. The differences are small enough that they may be a result of the simple explicit time-stepping routine or other modeling aspects (e.g., rounding the prescribed smoothed boundary layer depth z_i to the nearest grid level value). This is not contradicting the result of van Driel and Jonker (2011) considering that the afternoons studied here are 2 h or longer, and hence long in comparison to the large-eddy turn-over time of turbulence.

Our BLD runs showed an increase in midday TKE from about 0.8 to $1.3 \, \text{m}^2 \, \text{s}^{-2}$ for a change of prescribed boundary layer depth from 400 to 1600 m and smaller differences were observed at the end of the afternoon. Normalization of the modeled TKE with the mid-day TKE value (TKE_0) collapsed the data very well (not shown here, but to within 1 %) and therefore differences due to boundary layer depth (when about constant during the afternoon) are small in such a representation.

In the lower row of Fig. 12, we show the TKE from the test runs listed in Table 3 and in the upper row the results after normalization with afternoon length and midday TKE. From left to right the SH, U_c, U_{inc} and U_{dec} runs are shown. Starting with the SH runs, testing the variation in TKE due to changed sensible heat flux forcing, it is clear (from the lower left plot) that higher TKE levels are found in midday as a more convective boundary layer is modeled. From the upper left figure, it is also clear that the turbulence maintained by wind shear at the end of the afternoon becomes in percentage a smaller amount of the midday TKE value for increasingly convective conditions. Due to slight memory effects, the actual TKE level at the end of the afternoon can, however, be slightly higher in the convective simulations than in the completely neutral case with constant wind speed (full black line). The neutral case have a steady state TKE level due to a balance of shear production, transport and dissipation maintained throughout the simulations. This memory effect caused by convectively generated turbulence not being completely dissipated at the end of the afternoon is however small. In this case and this close to the surface it is less than 15 % of the TKE in the neutral simulation.

Turning now to the cases of U_c simulations where the wind speed is systematically increased from 0 to $3 \, \text{m} \, \text{s}^{-1}$ (second plot to the left in the lower row), TKE levels

increase with increasing wind speed, as expected. From the corresponding upper figure, it is also clear that percentage decay of TKE during the afternoon decreases with increasing wind speed. In the limit of very high and constant wind speed, we would (using this normalization) approach the neutral steady state solution where buoyancy flux no longer matters (corresponding to the zero buoyancy flux case of the upper left figure). Hence, it is the relative amount of shear and buoyancy that determines this decay percentage in the case of constant wind speed.

Results from the slightly more complicated situation of TKE evolution in the case of a linearly increasing wind speed during the afternoon from zero to a specified value at the end of the afternoon (U_{inc} runs) are shown in the lower second plot from the right in Fig. 12. The midday TKE level is the same as for the zero wind speed simulation, and successively increasing the wind speed decreases the turbulence decay for the afternoon. For the two windiest cases, an increase of TKE during the afternoon is observed instead of a decay. At the very end of the simulations, a slight drop in TKE can be seen even for these cases. This is due to a decrease in the stability corrected u_* value as we approach neutral conditions, but this effect is small compared to the general increase of TKE due to the increasing shear production. Normalization of these cases using a midday TKE value is shown in the upper figure. The normalization does not collapse the data simply because the midday TKE level was the same and it was the changes that occurred during the afternoon that caused the difference in TKE levels at the end of the afternoon.

Finally, in the plots on the right we show the results from our U_{dec} runs in which we decrease wind speed linearly to zero from some value (which was held constant up until midday). A decrease of wind speed is often the typical situation for variation of surface layer wind speed during the afternoon (Wingo and Knupp, 2015). In this case the midday value for TKE is the same as in our U_c runs, where wind speed was held constant throughout the entire simulation. The difference is that shear production decreases continuously during the afternoon and hence at the end of the afternoon there is no wind to maintain turbulence and significantly lower turbulence levels are

A simple TKE model

E. Nilsson et al.

Title Page

Abstract | Introduction

Conclusions | References

Tables | Figures

⏮ | ⏭

◀ | ▶

Back | Close

Full Screen / Esc

Printer-friendly Version

Interactive Discussion

found at the end of the afternoon. In this case, a normalization with the midday TKE value will of course cause a gathering of the curves, but the most windy midday situation (black full line), which has the largest change of production of TKE from midday until the end of afternoon, clearly has the fastest percentage decay of TKE. This situation was faster than the approximately linear decay seen for the simulation with $U_0 = 2\,\mathrm{m\,s}^{-1}$ marked with a dashed black line.

The result of an approximately linear decay of TKE in time can be very instructive to consider in relationship to previous modeling results from Nadeau et al. (2011), Sorbjan (1997), Nieuwstadt and Brost (1986). They chose to describe their results with a logarithmic representation for both TKE and time and discuss the turbulence decay in terms of a decay exponent parameter α such that a time dependence of normalized TKE is related to t^{α}. Whereas early LES studies (Nieuwstadt and Brost, 1986; Sorbjan, 1997) lead to decay exponents of –1.2 and –2, surface layer measurements (Nadeau et al., 2011) pointed out the existence of a range of exponents (e.g., –2 through at least –6). In the case of a linear change of TKE with time such that $\mathrm{TKE} = kt + \mathrm{TKE}_0$, we obtain $y = \ln(\mathrm{TKE}) = \ln(ke^x + \mathrm{TKE}_0)$ with $x = \ln(t)$ and the decay parameter then becomes: $\alpha = \frac{\partial y}{\partial x} = 1 - \frac{\mathrm{TKE}_0}{\mathrm{TKE}_0 + kt}$. This shows that α becomes a function of time for the simple case of a linear change of TKE with time. Furthermore, two values of observed α during a single afternoon such as –2 and –6 can occur without necessarily implying a different decay rate of TKE in terms of $\mathrm{m}^2\,\mathrm{s}^{-3}$ at those times. Therefore, and in the light of the above simulation results, which show both faster and slower than linear decay rates (and even increasing TKE for afternoons with increasing wind speed), we conclude that at heights near the surface there is unlikely any general simple decay exponent value α for turbulence kinetic energy.

To better understand our numerical model results for TKE, near the surface we can compare our numerical results to a simple analytical expression for TKE which comes from assuming quasi-stationarity such that $\frac{dE}{dt} \approx 0$ in Eq. (1). Additionally, we simplify the transport fraction T_f as 0.4, ignoring the weak dependence on atmospheric stratification such that about 0.6 times the total near-surface production is balanced by

local dissipation. We use Eqs. (3) and (4) together with the definition of friction velocity ($u_*^2 = -\overline{u'w'}$) for the shear production term, and the definition of convective velocity scale ($w_*^3 = \frac{gz_i}{\theta_v}(\overline{w'\theta_v'})_s$) for the buoyancy production term. Then, rearranging the TKE budget terms and solving for TKE from our dissipation parametrization (Eq. 16) yields:

$$E^{3/2} = \frac{0.6l_\epsilon u_*^3}{kz}\left(1 + 3.6k^{2/3}\left(\frac{z}{z_i}\right)^{2/3}\left(\frac{w_*}{u_*}\right)^2\right)^{-1/2} + \frac{0.6l_\epsilon w_*^3}{z_i}. \tag{20}$$

Here, also z/L in the wind gradient expression has been rewritten in terms of w_* and u_* using $\frac{z}{L} = \frac{-kzw_*^3}{z_i u_*^3}$ (Stull, 1988) as it may be more instructive to consider how TKE in this simplified analytical expression is influenced by these governing velocity scales. This equation becomes a function of u_*, z and z_i when w_* is small and conversely a function of w_*, z and z_i when u_* is small, which seems reasonable. The influence of z_i on near surface TKE may be questionable, but it is consistent with our findings from Part 1 and z_i used by Nadeau et al. (2011). A comparison is shown in Fig. 13 between numerically modeled TKE and TKE determined from Eq. (20) for the simulation results shown in Fig. 12. It is clear that the simplified equation is within about 10 % of the numerical model results for TKE (at worst and often better) at this near-surface height of 2 m.

In Fig. 14 (left panel), the simplified analytical expression is used to illustrate the dependence of TKE on w_* for five different values of u_* (green colored lines) and a fixed boundary layer depth of 750 m. The plot also shows hourly data from the afternoon period with different colored symbols for the different days. The color scheme for the data is consistent with Part 1. That is, windier afternoons are shown in magenta, while the lowest wind speeds are shown in light blue. The results indicate that the simple expression for TKE variation is consistent with the observed trend of increasing TKE for increasing wind speed and u_* and reverts back to a w_* only expression for zero u_*. Included in the figure is also a simple linear fit between observed TKE and w_* as a dashed black line ignoring the observed trend in u_*.

The middle panel of Fig. 14 shows TKE calculated by this simple linear fitted expression (TKE $= 0.1w_*^2 + 0.75$) using the observed w_* compared to the observed TKE. This is done to provide a very simple reference model (or fit) to have something to compare calculated evaluation metrics for Eq. (20) with. It is seen that the variability of calculated TKE from our simple linear fit is lower than in the observed data. Days with low wind over predicts TKE, while days with stronger winds under predict TKE.

The right panel of Fig. 14 shows TKE calculated from Eq. (20) and observed TKE. Here, we used the observed z_i and u_* in addition to the observed w_* (as was also done for the simple linear fitted model). The figure shows that the variability of predicted TKE is larger than the observed TKE. Evidently, sometimes u_* observations have large hourly variability, which is not always linked to a large increase or decrease in TKE. For example, on 20 June (Fig. 8) there is one hour with observed $u_* > 0.3$ that is significantly higher than the surrounding hours when $u_* \approx 0.22$. This is the hour that leads to the highest predicted TKE value when using Eq. (20) and has the largest individual hourly error. It is also possible that the analytical model is somewhat overly sensitive to some of the input parameters, contributing to variability in TKE that exceeds the observations. Windier afternoons appear to be associated with an over prediction of TKE, while those with very weak winds under predict TKE somewhat. These trends, however, are not as clear as for the simple linear-fit model which takes into account of only w_*.

It is not possible to conclude with the evaluation metrics used here whether the TKE prediction was improved by including u_* compared to an expression that only uses w_*. However, since Eq. (20) is based on relevant scaling variables, we consider it preferable to the empirical linear fit. The model presented here is also consistent with the observed TKE budget at the Divergence site during the BLLAST field campaign, but should obviously be further tested on other sites and data before any conclusion on general validity can be made.

7   Discussion and conclusions

This study presents a simple one-dimensional model to investigate atmospheric turbulence kinetic energy in sheared convective boundary layers. Similar to a previously proposed heuristic model for the surface layer TKE decay (Nadeau et al., 2011), our
5   model uses boundary layer depth and buoyancy flux as input variables. However, we also include near-surface wind speed to handle less convectively forced situations. The model is based on a simplified TKE budget including idealized height-varying terms for shear production, buoyant production, transport and dissipation, which together with initial conditions, provides a basis for the evolution of TKE during the unstable part of
10   the day until the start of stable conditions.

In the present work, the model was first run constrained by observations from the BLLAST field campaign for nine IOP days with relatively successful results for a near-surface TKE observed at 2.23 m. Further above the ground, results were not as good, but still quite reasonable (illustrated by measurements at 61.4 m). The height
15   dependence of each budget term and therefore TKE can be challenging to model correctly. This was illustrated by the shear production term being rather well predicted near the surface, but its performance degraded with height. This height dependence of shear production proved difficult to infer from a single height wind measurement and further work is required to improve upon this model deficiency. Also, the model is
20   unable to capture all the hourly variability observed in TKE budget terms and TKE. As long as no large systematic errors occur over extended periods of time, the mean TKE level is, however, quite well-predicted by the model in many situations for these 9 days. As discussed in Part 1, the nine studied days include a variety of atmospheric stability conditions. The fact that the model is able to simulate roughly the right magnitude and
25   temporal variations of near surface TKE, both on more convective days and in more sheared conditions (e.g. 26 June), supports that the budget relationships presented in Part 1 are realistic and can be used for atmospheric modeling applications and explorations.

The simple TKE model with all its discussed deficiencies still often yields quite realistic predictions of the overall evolution of boundary layer TKE and dissipation rate throughout the ABL depth. Further evaluation and investigation into the differences between the model and observations (as well as differences between different instrument estimates) may be needed. Currently, the model tends to predict quite high TKE dissipation rates when forced by observations from a forest site and wheat field. Also, using a $2\,km \times 2\,km$ area averaged flux gives modeled TKE dissipation rates, which are high compared to observations. This is probably partly due to modeling uncertainties of urban and bare-soil conditions where no measurements were available. Observed dissipation rates are often lower than in the model. Elevated shear and the effects of different entrainment rates on different days may also be very important.

The model was used to illustrate its usefulness in understanding afternoon transition physics. The simple model was used to identify a region of reduced turbulence that starts in the upper parts of the boundary layer (but below the capping inversion), which moves down with time toward the surface. This phenomena was conceptually described as a pre-residual layer. The pre-residual layer is consistent with the conclusions from Darbieu et al. (2015) who noted that changes occur first in the upper part of the boundary layer during the later stages of the afternoon transition. In the pre-residual layer, there is evidence that turbulence characteristics change as the layer forms with weak turbulence aloft, while the surface is still unstable. The process occurring during this time period influence the onset conditions for the actual residual layer, which resides entirely above the stable boundary layer. Further work should attempt to better understand the role of the pre-residual layer.

The model was further used in idealized setting to illustrate the effects of relative amounts of shear and buoyancy for near-surface TKE at a height of $2\,m$. It was illustrated that many different decay rates can exist in the afternoon. Both faster and slower than linearly decaying TKE was possible when the model was driven with a simple time-varying wind. For a linearly increasing wind speed throughout the

afternoon, TKE may increase during the afternoon despite a decrease of buoyancy production during the afternoon depending on shear production levels. This was also observed on 27 June as discussed in Part 1. We also found that a linear decrease of TKE during an afternoon leads to a decay exponent value that is time-dependent and that no unique scaling law exponent exists in this situation.

We simplified our numerical model results to an analytical expression for quasi-stationary near-surface turbulence in Eq. (20). It compared well with the numerical results and was shown to reduce to an expression involving only w_* as the relevant velocity scale in the case of zero friction velocity. And, conversely to an expression involving only u_* as the relevant velocity scale in the case of zero w_*. Both these cases are somewhat irrelevant for the atmospheric case in general because there will usually be some small amount of shear and buoyancy present. The fact that our numerical and analytical results compared relatively well indicates the usefulness of the quasi-stationarity assumption when describing the observed slow trends in the evolution of TKE. Further studies are, however, needed about the more rapid variations of TKE that occur on shorter time scales when also forcing time scales becomes comparable to large eddy turn-over time scales (van Driel and Jonker, 2011). In future work we should also confront our model with an LES model that uses the same measured fluxes as lower boundary conditions.

In reality, atmospheric turbulence kinetic energy is governed by many parameters some of which have been included in the presented numerical model for TKE and others such as horizontal advection and elevated wind shear which remains to be included. In addition, TKE also has some memory of the history of the flow that we neglect when using Eq. (20). It should therefore be used with caution for prediction of turbulence kinetic energy. There is also no reason to be certain that for instance the near-surface transport fraction of about 0.4 determined from our measurements need to apply to other datasets. The methodology from which our model originates we argue, however, is reasonably general and may be attempted in future work also on other sites and in other conditions.

Appendix A: Summary of model of height variation of TKE budget from Lenschow (1974)

For a qualitative comparison to our proposed height variation of TKE budget terms we provide here the simple model from Lenschow (1974). They discuss a turbulence kinetic energy equation normalized by buoyancy flux, and express it as

$$H + T_r + S - D = 0,$$ (A1)

where H and S are the buoyancy- and shear-generation terms, T_r the divergence of the vertical transport of turbulence energy and pressure fluctuations, and D the dissipation rate.

Their expression for buoyancy production is given by

$$H = 1 - 1.15(z/z_i),$$ (A2)

for $z/z_i \leq 0.87$, and for $0.87 \leq z/z_i \leq 1$ they instead use

$$H = -13.81 + 49.96(z/z_i) - 58.78(z/z_i)^2 + 22.53(z/z_i)^3.$$ (A3)

For shear production they use

$$S = -\frac{L}{z_i}\left(1 - 15\frac{z_i}{L}\frac{z}{z_i}\right)^{-1/4}.$$ (A4)

For dissipation rate their expression is

$$D = 0.43 + \frac{0.57}{\langle S \rangle + 3.75}\left(\langle S \rangle - S\right) + S,$$ (A5)

where $\langle S \rangle$ is an integrated shear production over the boundary layer depth given by

$$\langle S \rangle = -\frac{L}{z_i}\left[ln\frac{z}{z_0} - \psi_1(x)\right],$$

under the assumption of a constant shear stress throughout the surface and mixed layer. Here

$$x = (1 - 15z_i/L)^{1/4},$$

$$\psi_1(x) = 2\ln\frac{1+x}{2} + \ln\frac{1+x^2}{2} - 2\tan^{-1}x + \pi/2.$$

And for transport they use

$$T_r = 0.43 + \frac{0.57}{\langle S \rangle + 3.75}\left(\langle S \rangle - S\right) - H. \tag{A6}$$

This model from Lenschow (1974) is illustrated for a more convective case ($z_i/L = -1000$) in Fig. A1 and for a more neutral case ($z_i/L = -1$) in Fig. A2. See Sect. 3.3 for discussions concerning the vertical profiles of TKE budget terms in this model in relationship to our TKE model.

It is worth to note again here, however, that TKE tendency is assumed to be exactly zero in Lenschow (1974) and no prediction of TKE is therefore provided by this model. Also no expressions are provided for the TKE budget terms above the boundary layer depth (defined as height of minimum buoyancy flux). In the case of near neutral stratification it is also clear from Fig. A2 that the transport term (dash-dotted line) becomes very small in this model in comparison to the total turbulence production, which in this case is completely dominated by shear production (dashed line). Thereby the dissipation term becomes more dominant in these conditions for the model from Lenschow (1974) in comparison to our model. Our model uses a near-surface transport fraction of about 0.36 in neutral conditions and 0.46 in very convective conditions (see Fig. 5 and Eq. 15). For comparison the model from Lenschow (1974) obtains a near-surface transport fraction value for very convective conditions of 0.57. See also discussion in Part 1 that data from Dupuis et al. (1997) may suggest a value as large as 0.69 in convective conditions. Further study may therefore be needed to explore the typical range of this parameter on different sites and in different conditions.

References

Basu, S., Vinuesa, J., and Swift, A.: Dynamic LES modeling of a diurnal cycle, J. Appl. Meteorol. Clim., 47, 1156–1174, 2008. 29810

Beare, R. J., Edwards, J. M., and Lapworth, A.: Simulation of the observed evening transition and nocturnal boundary layers: large-eddy simulation, Q. J. Roy. Meteor. Soc., 132, 81–99, 2006. 29810

Blay-Carreras, E., Pino, D., Van de Boer, A., De Coster, O., Darbieu, C., Hartogensis, O., Lohou, F., Lothon, M., Pietersen, H., and Vilà-Guerau de Arellano, J.: Role of the residual

ACPD

15, 29807–29869, 2015

A simple TKE model

E. Nilsson et al.

Title Page

Abstract | Introduction

Conclusions | References

Tables | Figures

|◄ | ►|

◄ | ►

Back | Close

Full Screen / Esc

Printer-friendly Version

Interactive Discussion

layer and large-scale subsidence on the development and evolution of the convective boundary layer, Atmos. Chem. Phys. Discuss., 13, 31527–31562, doi:10.5194/acpd-13-31527-2013, 2013. 29810

BLLAST: Boundary Layer Late Afternoon and Sunset Turbulence (BLLAST) website, available at: http://bllast.sedoo.fr/database/ (last access: 10 October 2015), 2015. 29813

Brown, A., Cederwall, R., Chlond, A., Duynkerke, P., Golaz, J., Khairoutdinov, M., Lewellen, D., Lock, A., MacVean, M., Moeng, C.-H., R. A. J., N., Siebsma, A., and Stevens, B.: Large-eddy simulation of the diurnal cycle of shallow cumulus convection over land, Q. J. Roy. Meteor. Soc., 128, 1075–1093, 2002. 29810

Couvreux, F., Bazile, E., Canut, E., Seity, Y., Lothon, M., Lohou, F., Guichard, F., and Nilsson, E.: Boundary-layer turbulent processes and mesoscale variability represented by Numerical Weather Prediction models during the BLLAST campaign, Atmos. Chem. Phys. Discuss., in press, 2015. 29810, 29833

Darbieu, C., Lohou, F., Lothon, M., Vilà-Guerau de Arellano, J., Couvreux, F., Durand, P., Pino, D., Patton, E. G., Nilsson, E., Blay-Carreras, E., and Gioli, B.: Turbulence vertical structure of the boundary layer during the afternoon transition, Atmos. Chem. Phys., 15, 10071–10086, doi:10.5194/acp-15-10071-2015, 2015. 29810, 29820, 29833, 29842, 29855

De Coster, O. and Pietersen, H.: BLLAST – Uniform Processing of Eddy-Covariance Data, available at: http://bllast.sedoo.fr/documents/reports/H-Pietersen_O-de-Coster_BLLAST-surf_flx-uniform-processing.pdf, last access: 10 October 2015, 2012. 29813

Deardorff, J.: Numerical investigation of neutral and unstable planetary boundary layers, J. Atmos. Sci., 29, 91–115, 1972. 29820

Dupuis, H., Taylor, P. K., Weill, A., and Katsaros, K.: Inertial dissipation method applied to derive turbulent fluxes over the ocean during the Surface of the Ocean, Fluxes and Interactions with the Atmosphere/Atlantic Stratocumulus Transition Experiment (SOFIA/ASTEX) and Structure des Echanges Mer-Atmosphere, Proprietes des Heterogeneites Oceaniques: Recherche Experimentale (SEMAPHORE) experiments with low to moderate wind speeds, J. Geophys. Res., 102, 21115–21129, 1997. 29824, 29845

Emanuel, K. A.: Atmospheric convection, Oxford University Press, New York, 580 pp, 1994. 29809

Garcia, D.: Robust smoothing of gridded data in one and higher dimensions with missing values, Comput. Statist. Data Anal., 54, 1167–1178, 2010. 29815

A simple TKE model

E. Nilsson et al.

Title Page

Abstract	Introduction
Conclusions	References
Tables	Figures

◀ | ▶

◀ | ▶

Back | Close

Full Screen / Esc

Printer-friendly Version

Interactive Discussion

Garratt, J.: The Atmospheric Boundary Layer, Cambridge University Press, Cambridge, UK, 316 pp., 1992. 29813

Goulart, A., Degrazia, G., Rizza, U., and Anfossi, D.: A theoretical model for the study of convective turbulence decay and comparison with large-eddy simulation data, Bound.-Lay. Meteorol., 107, 143–155, 2003. 29810

Goulart, A., Bodmann, B., de Vilhena, M., Soares, P., and Moreira, D.: On the time evolution of the turbulent kinetic energy spectrum for decaying turbulence in the convective boundary layer, Bound.-Lay. Meteorol., 138, 61–75, 2010. 29810

Grimsdell, A. W. and Angevine, W. M.: Observations of the afternoon transition of the convective boundary layer, J. Appl. Meteorol., 41, 3–11, 2002. 29832

Hartogensis, O. K.: BLLAST Flux Maps, available at: http://bllast.sedoo.fr/workshops/february2015/presentations/Hartogensis-Oscar_area-averaged-flux.pdf (last access: 10 October 2015), 2015. 29813, 29830, 29831, 29832

Högström, U.: Non-dimensional wind and temperature profiles in the atmospheric surface layer, Bound.-Lay. Meteorol., 42, 263–270, 1988. 29817

Jacoby-Koaly, S., Campistron, B., Bernard, S., Bénech, B., Ardhuin-Girard, F., Dessens, J., Dupont, E., and Carissimo, B.: Turbulent dissipation rate in the boundary layer via UHF Wind Profiler Doppler Spectral Width Measurements, Bound.-Lay. Meteorol., 103, 361–389, 2002. 29815

Kumar, V., Kleissl, J., Meneveau, C., and Parlange, M.: Large eddy simulation of a diurnal cycle of the atmospheric boundary layer: atmospheric stability and scaling issues, Water Resour. Res., 42, 3–18, 2006. 29810

Lenschow, D., Wyngaard, J., and Pennel, W.: Mean-field and second-moment budgets in a baroclinic, convective boundary layer, J. Atmos. Sci., 37, 1313–1326, 1980. 29819

Lenschow, D. H.: Model of height variation of the Turbulence Kinetic Energy budget in the unstable planetary boundary layer, J. Atmos. Sci., 31, 465–474, 1974. 29820, 29821, 29824, 29825, 29844, 29845, 29868, 29869

Lothon, M., Lohou, F., Pino, D., Couvreux, F., Pardyjak, E. R., Reuder, J., Vilà-Guerau de Arellano, J., Durand, P., Hartogensis, O., Legain, D., Augustin, P., Gioli, B., Faloona, I., Yagüe, C., Alexander, D. C., Angevine, W. M., Bargain, E., Barrié, J., Bazile, E., Bezombes, Y., Blay-Carreras, E., van de Boer, A., Boichard, J. L., Bourdon, A., Butet, A., Campistron, B., de Coster, O., Cuxart, J., Dabas, A., Darbieu, C., Deboudt, K., Delbarre, H., Derrien, S., Flament, P., Fourmentin, M., Garai, A., Gibert, F., Graf, A.,

Title Page

Abstract | Introduction

Conclusions | References

Tables | Figures

|◄ | ►|

◄ | ►

Back | Close

Full Screen / Esc

Printer-friendly Version

Interactive Discussion

Groebner, J., Guichard, F., Jimenez Cortes, M. A., Jonassen, M., van den Kroonenberg, A., Lenschow, D. H., Magliulo, V., Martin, S., Martinez, D., Mastrorillo, L., Moene, A. F., Molinos, F., Moulin, E., Pietersen, H. P., Piguet, B., Pique, E., Román-Cascón, C., Rufin-Soler, C., Saïd, F., Sastre-Marugán, M., Seity, Y., Steeneveld, G. J., Toscano, P., Traullé, O., Tzanos, D., Wacker, S., Wildmann, N., and Zaldei, A.: The BLLAST field experiment: Boundary-Layer Late Afternoon and Sunset Turbulence, Atmos. Chem. Phys. Discuss., 14, 10789–10852, doi:10.5194/acpd-14-10789-2014, 2014. 29813, 29815, 29826, 29832, 29851

Mangia, C., Degrazia, G. A., and Rizza, U.: An integral formulation for the dispersion parameters in a Shear-Buoyancy-driven planetary boundary layer for use in a Gaussian Model for tall stacks, J. Appl. Meteorol., 39, 1913–1922, 2000. 29822

Nadeau, D. F., Pardyjak, E. R., Higgins, C. W., Fernando, H. J. S., and Parlange, M. B.: A simple model for the afternoon and early evening decay of convective turbulence over different land surfaces, Bound.-Lay. Meteorol., 141, 301–324, 2011. 29809, 29810, 29811, 29838, 29839, 29841

Nieuwstadt, F. T. M. and Brost, R. A.: The decay of convective turbulence, J. Atmos. Sci., 43, 532–546, 1986. 29809, 29838

Nilsson, E., Lohou, F., Lothon, M., Pardyjak, E., Mahrt, L., and Darbieu, C.: Turbulence Kinetic Energy budget during the afternoon transition – Part 1: Observed surface TKE budget and Boundary layer description for 10 Intensive Observation Period days, Atmos. Chem. Phys. Discuss., 15, 29747–29805, doi:10.5194/acpd-15-29747-2015, 2015. 29809

Pietersen, H., Vilà-Guerau de Arellano, J., Augustin, P., de Coster, O., Delbarre, H., Durand, P., Fourmentin, M., Gioli, B., Hartogensis, O., Lothon, M., Lohou, F., Pino, D., Ouwersloot, H. G., Reuder, J., and van de Boer, A.: Study of a prototypical convective boundary layer observed during BLLAST: contributions by large-scale forcings, Atmos. Chem. Phys. Discuss., 14, 19247–19291, doi:10.5194/acpd-14-19247-2014, 2014. 29810

Pino, D., Jonker, H. J. J., Vilà de Arellano, J., and Dosio, A.: Role of shear and the inversion strength during sunset turbulence over land: characteristic length scales, Bound.-Lay. Meteorol., 121, 537–556, 2006. 29809, 29810

Rizza, U., Miglietta, M., Degrazia, G., Acevedo, O., and Marques, E.: Sunset decay of the convective turbulence with Large-Eddy Simulation under realistic conditions, Physica A, 392, 4481–4490, 2013. 29810

Title Page

Abstract | Introduction

Conclusions | References

Tables | Figures

|◄ | ►|

◄ | ►

Back | Close

Full Screen / Esc

Printer-friendly Version

Interactive Discussion

Sorbjan, Z.: Decay of convective turbulence revisited, Bound.-Lay. Meteorol., 82, 501–515, 1997. 29809, 29834, 29838

Stull, R. B.: An Introduction to Boundary Layer Meteorology, Kluwer Academic Publishers, Dordrecht, the Netherlands, 666 pp., 1988. 29839

Van Dijk, A., Moene, A. F., and De Bruin, H. A. R.: The principles of surface flux physics: theory, practice and description of the ECPACK library, Internal Report 2004/1, Meteorology and Air Quality Group, Wageningen University, Wageningen, the Netherlands, 99 pp., 2004. 29813

van Driel, R. and Jonker, H. J. J.: Convective boundary layers driven by nonstationary surface heat fluxes, J. Atmos. Sci., 68, 727–738, 2011. 29809, 29836, 29843

Verkaik, J. and Holtslag, A. A. M.: Wind profiles, momentum fluxes and roughness lengths at Cabauw revisited, Bound.-Lay. Meteorol., 122, 701–719, 2007. 29821

Wilson, K.: An alternative function for the wind and temperature gradients in unstable surface layers, Bound.-Lay. Meteorol., 99, 151–158, 2001. 29817

Wingo, S. M. and Knupp, K. R.: Multi-platform observations characterizing the afternoon-to-evening transition of the planetary boundary layer in northern Alabama, USA, Bound.-Lay. Meteorol., 155, 29–53, 2015. 29837

Wyngaard, J. C.: Turbulence in the Atmosphere, Cambridge University Press, New York, 393 pp., 2010. 29821

Title Page

Abstract | Introduction

Conclusions | References

Tables | Figures

|◄ | ►|

◄ | ►

Back | Close

Full Screen / Esc

Printer-friendly Version

Interactive Discussion

Title Page

Abstract | Introduction

Conclusions | References

Tables | Figures

◄ | ►

Back | Close

Full Screen / Esc

Printer-friendly Version

Interactive Discussion

Table 1. Brief description of BLLAST measurement sites and data sets with the required buoyancy flux, winds and temperature for the modeling of TKE. Also listed are the roughness length (z_0) and displacement height (d) values in the model. For additional details see Lothon et al. (2014).

Name	Height [m a.s.l.]	Height [m a.g.l.]	Sampling rate [Hz]	Aver. period [min]	z_0 [m]	Disp. height d [m]
Divergence site	591	(2.23, 3.23, 5.27, 8.22)	20	10	0.02	0
60 m tower	602	(29.3, 45.8, 61.4)	10	10	–	–
Grass site	580	2.55	20	30	0.02	0
Corn site	645	2.93	20	30	0.02	0
Moor site	641	2.93	20	30	0.02	0
Wheat site	582	3.0	20	30	0.02	0
Forest site (Pine)	620	31.55	10	30	0.2	$\frac{2}{3}$ 20
2 km × 2 km	–	8.22 (for wind speed)	–	30	0.02	0

Full Screen / Esc

Printer-friendly Version

Interactive Discussion

Table 2. Simulation settings for model experiment test runs.

Name	Parameter	Reference run	AL runs	BLD runs
Afternoon length	τ_{cos} [h]	6	(2, 4, 6, 8, 10)	6
Maximum sensible heat flux	H_{max} [W m^{-2}]	200	200	200
Wind speed at 10 m	U_{10} [m s^{-1}]	$U_{mean} = 2.0$	$U_{mean} = 2.0$	$U_{mean} = 2.0$
Afternoon boundary layer depth	$z_{i_{max}}$ [km]	1.0	1.0	(0.4, 0.6, 0.8, 1.0, 1.2, 1.4, 1.6)

Table 3. Simulation settings for model experiment test runs.

Parameter	SH runs	U_c runs	U_{inc} runs	U_{dec} runs
τ_{cos} [h]	6	6	6	6
H_{max} [W m^{-2}]	(0, 50, 100, 150, 200, 300, 400, 500)	200	200	200
U_{10} [m s^{-1}]	$U_{mean} = 2.0$	$U_{c*} = (0, 0.5, 1, 1.5, 2.0, 2.5, 3.0)$	$U_1 = U_{c*}$	$U_0 = U_{c*}$
$z_{i_{max}}$ [km]	1.0	1.0	1.0	1.0

Title Page

Abstract | Introduction

Conclusions | References

Tables | Figures

|◀ | ▶|

◀ | ▶

Back | Close

Full Screen / Esc

Printer-friendly Version

Interactive Discussion
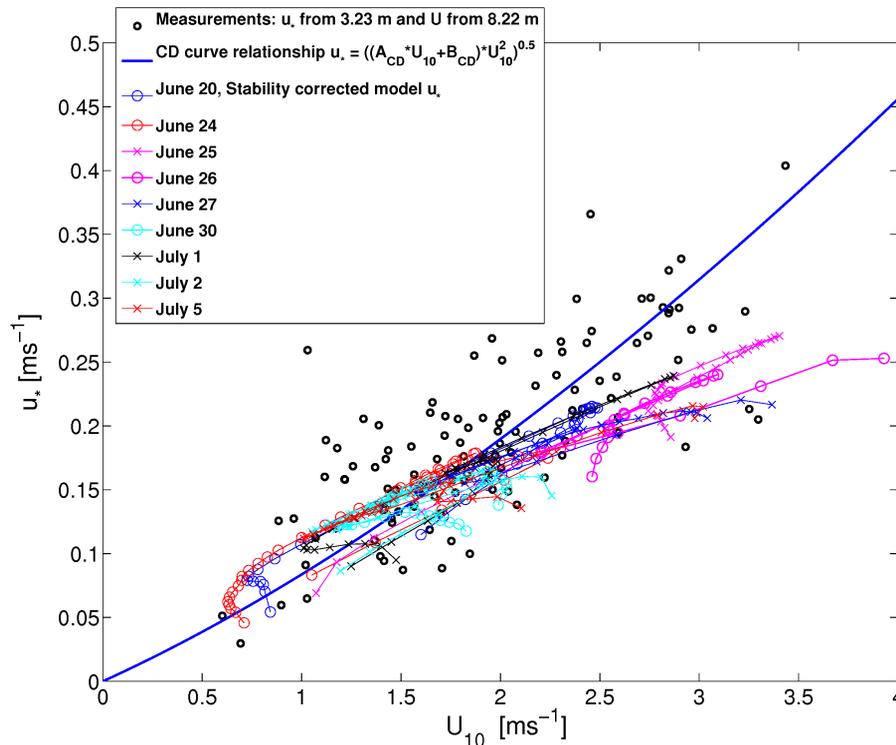
Figure 1. Measured hourly averaged u_* from the 3.23 m level is shown as a function of wind speed at 8.22 m in black circles. The model u_* prediction from a simple CD curve relationship with $A_{CD} = 2 \times 10^{-3}\,\mathrm{s\,m^{-1}}$ and $B_{CD} = 5 \times 10^{-3}$ (unitless) is shown as a blue line. The model stability corrected u_* values for 9 IOP days are also shown in different colored lines with circles or crosses as a function of the 10 m model wind speed for every 20 min during the simulations.
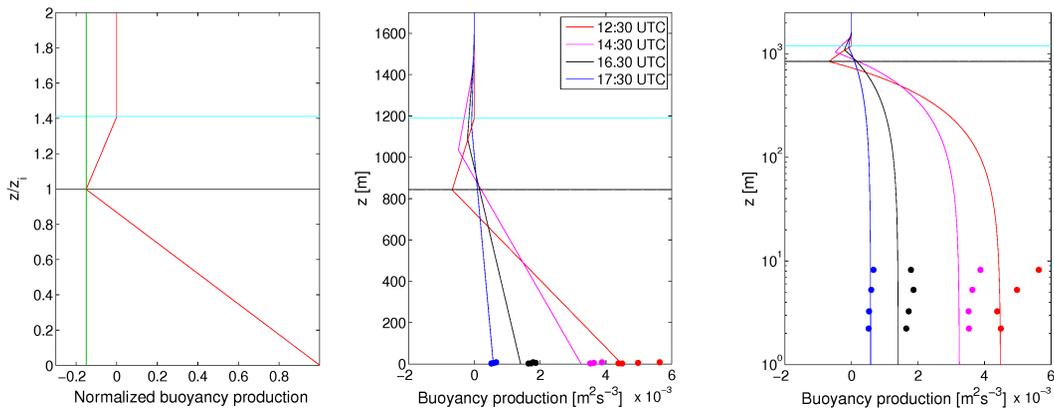
Figure 2. The left panel shows the simple modeled height dependence for the buoyancy production term in the TKE budget normalized by the surface value (in red). A vertical green line is added at −0.15, which is the entrainment parameter value in the model taken from the large-eddy simulation of 20 June (Darbieu et al., 2015). A horizontal black line indicates the boundary layer depth z_i defined from smoothed lidar measurements whereas the horizontal light blue line indicates z_{i0}, the height of no turbulence. The middle panel shows an example of the evolution of the vertical profiles during the afternoon of 20 June. Measurements corresponding to the hourly averaged budget results for the four heights on the small tower are shown as colored dots. Boundary layer height z_i and height of no turbulence z_{i0} for 12:30 UTC are shown as horizontal black and light blue line. The right panel corresponds to the middle panel, but shows the model and data on a semi-logarithmic scale to better display the near surface behavior.
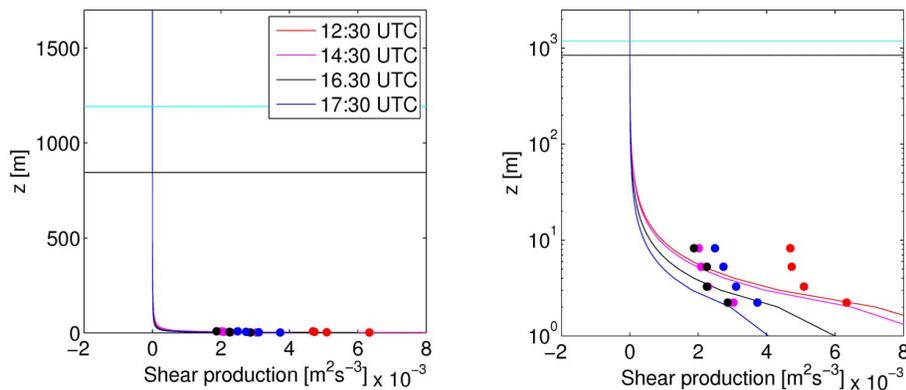
Figure 3. (Left panel) Modeled (in lines) and observed (in dots) shear production for the afternoon of 20 June. Red, magenta, black and blue colors correspond to 12:30, 14:30, 16:30 and 17:30 UTC respectively. Horizontal black lines correspond to boundary layer depth z_i and the light blue horizontal line to height of no turbulence z_{i0} at 12:30 UTC. The right panel shows the model and data in a semi-logarithmic representation to better display the near surface behavior.
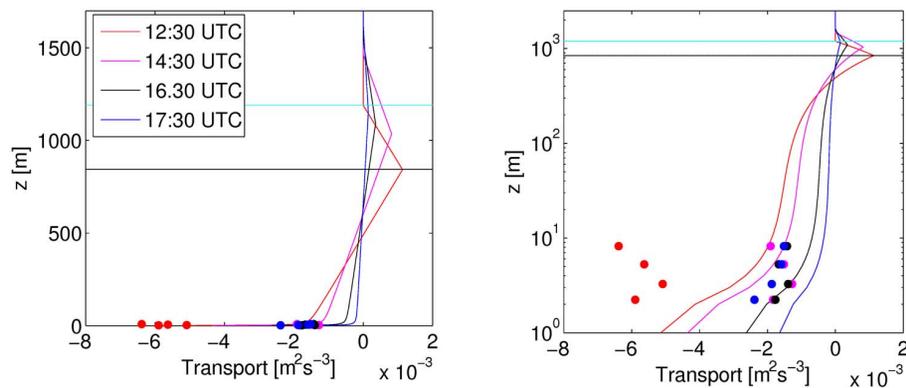
Figure 4. Same as Fig. 3 but for the transport term of the TKE budget.
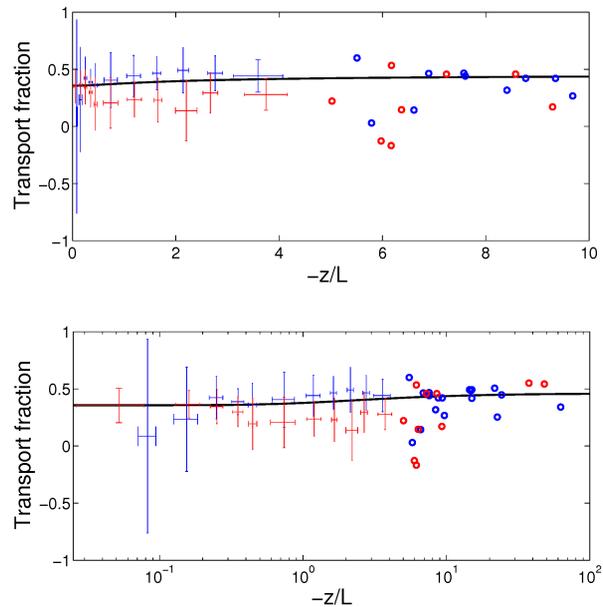
Figure 5. Near surface transport fraction defined as minus the ratio of the total transport term to the sum of buoyancy and shear production. Red circles show hourly averaged data from the afternoon period from 12:00 UTC to zero buoyancy flux for $z/L > 5$ when data are sparse. Blue circles show the corresponding data from the morning period from positive sensible heat flux up until 12:00 UTC. The data coverage is successively better for more neutral stabilities and we show averaged data with error bars corresponding to ±1 standard deviation for both afternoon and morning period data for different intervals of the stability parameter z/L. The intervals used have sizes of $0.1z/L$ for $z/L < 1.0$, $0.5z/L$ for $1 < z/L < 3$ and one additional interval $3 < z/L < 5$ is also included. The lower figure corresponds to the upper, but with a logarithmic abscissa to better display the very near-neutral data and to also include a few hours with z/L values above 10. In both figures, the model expression for transport fraction, which is applied at the first gridpoint (1 m above the surface) is included as a black line.
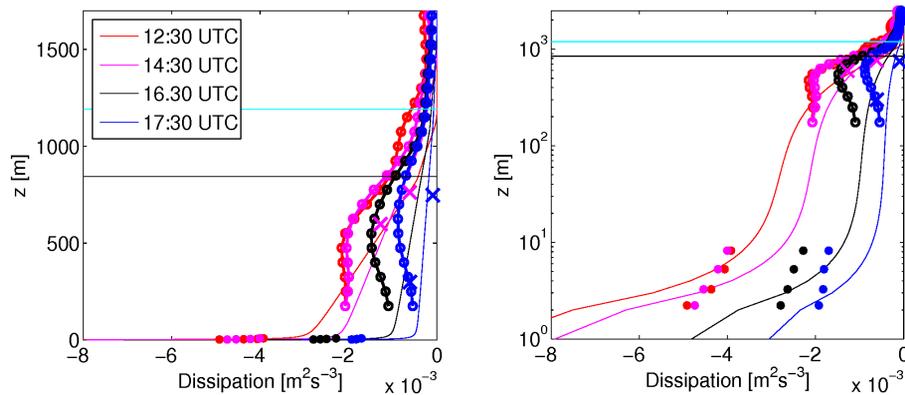
Figure 6. Same as Fig. 3 but for the dissipation term of the TKE budget. Here, smoothed and hourly averaged dissipation estimates are also included from the UHF wind profiler from 175 m (lines with circles). Estimates of dissipation from the Piper Aztec aircraft are included as colored crosses. Here, all aircraft flight legs during one hour centered on 14:30 and 17:30 UTC respectively were averaged for height intervals of 75 m.
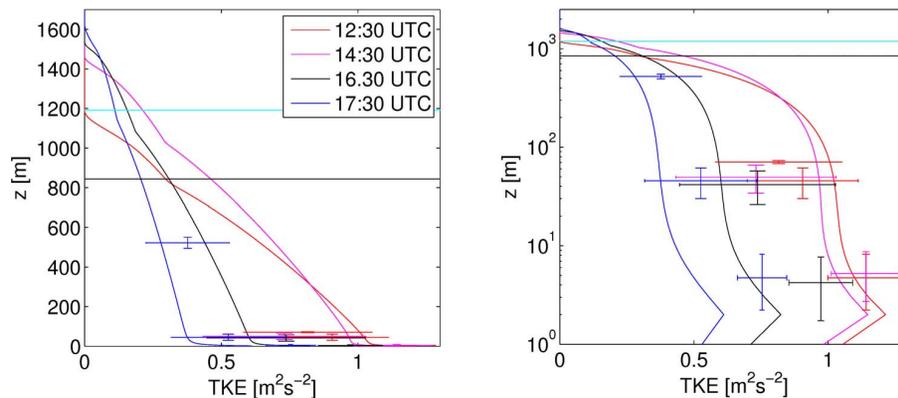
Figure 7. Profiles of TKE during the afternoon period on 20 June. The color scheme is the same as in earlier figures. The measurements on both the small tower (2–8 m) and the taller 60 m tower (30–60 m) were averaged and are shown with one ±1 standard deviation. The data at times 14:30 and 16:30 UTC were displaced slightly in height to more easily see all error bars. The vertical error bar denote upper and lower height limits of data. Also included (at 12:30 and 17:30 UTC) is TKE from a tethered balloon-borne 3-D sonic operating at about 70 and 520 m respectively.
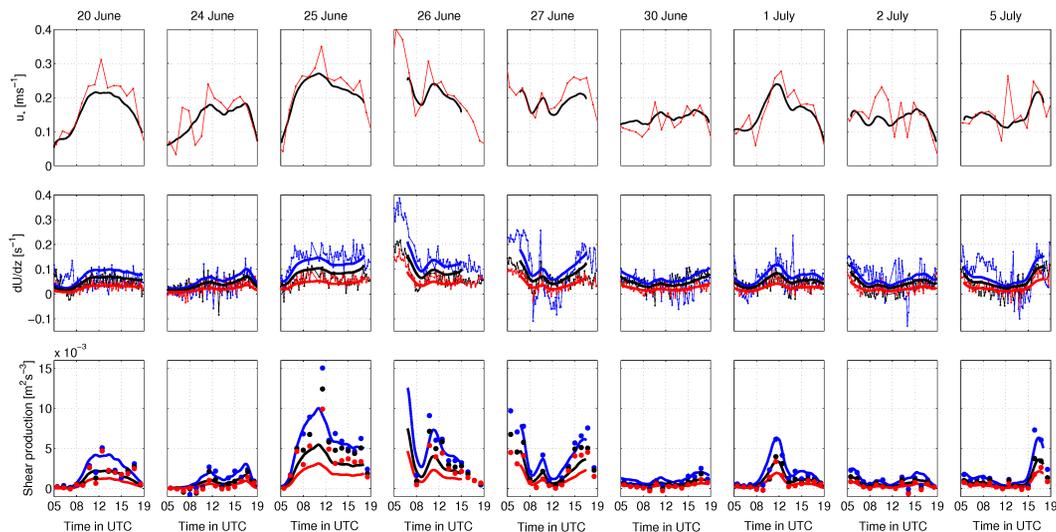
Figure 8. The upper row shows the modeled stability corrected friction velocity (black line) and observations at 3.23 m (red line with dots) for 9 simulated days. The simulations are performed only for unstable conditions whereas measurements are shown between 05:00 and 19:00 UTC on all days. The middle row shows the measured wind gradient at 2.73, 4.23, 6.75 m as thin blue, black and red line with dots and the corresponding modeled wind gradients is shown as full blue, black and red line for the 3, 4 and 7 m model levels. The lower row shows the modeled shear production interpolated to the measurement heights of the three upper levels on the small tower as full lines. The corresponding hourly budget shear production values are shown as blue, black and red filled circles when available under the conditions discussed in Part 1. The shear production term is temporarily both over and underestimating with a clear tendency to underestimate especially at 8.22 m for conditions with higher observed shear production.
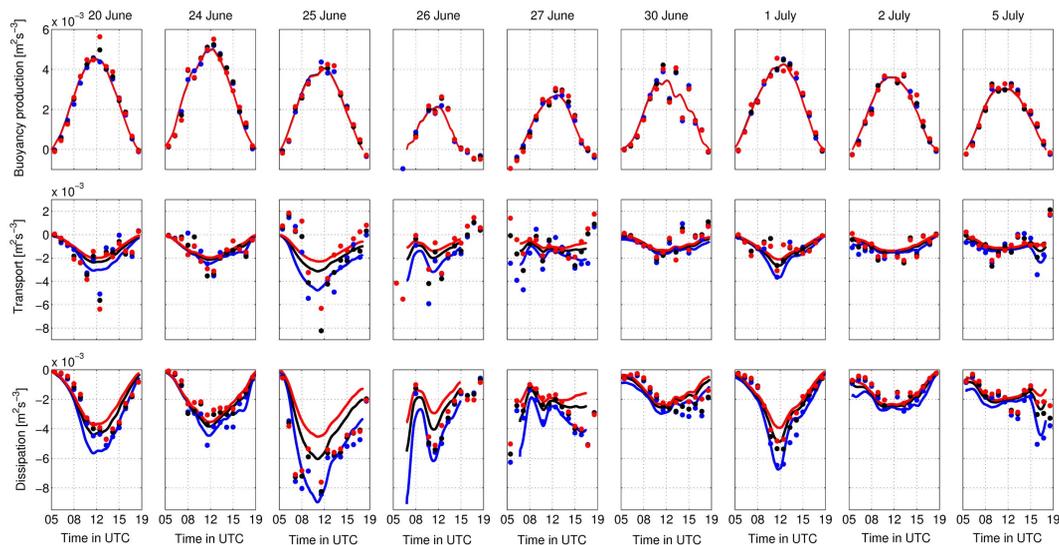
Figure 9. The upper row shows the observed hourly averaged buoyancy production at 2.23, 5.27, 8.22 m (filled blue, black and red circles) and the corresponding model buoyancy production (lines) with very small height variation. The middle row shows the corresponding observed and modeled values for transport with larger scatter in observed values and larger discrepancies between model and measurements for some time periods and days. The lower row shows the corresponding observed and modelled values of dissipation, which tend to underestimate dissipation at 8.22 m when shear production is larger.

Full Screen / Esc

Printer-friendly Version

Interactive Discussion
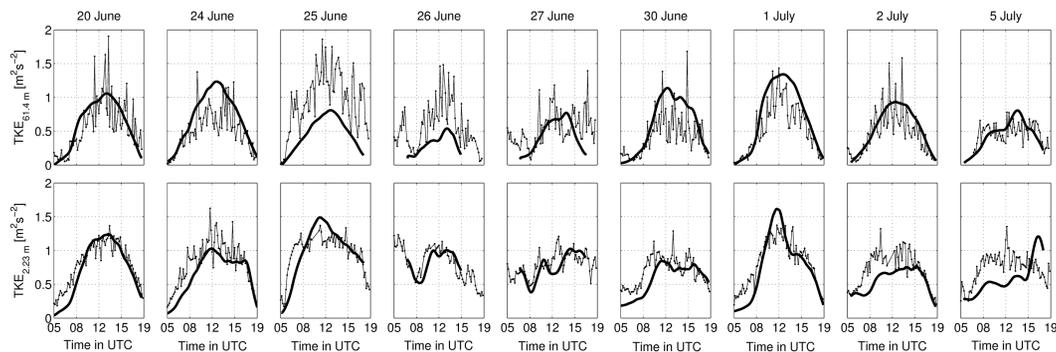
Figure 10. The lower row shows the modeled TKE interpolated to 2.23 m (full lines) and observations (thin lines with dots). The upper row shows TKE at the 61.4 m level.
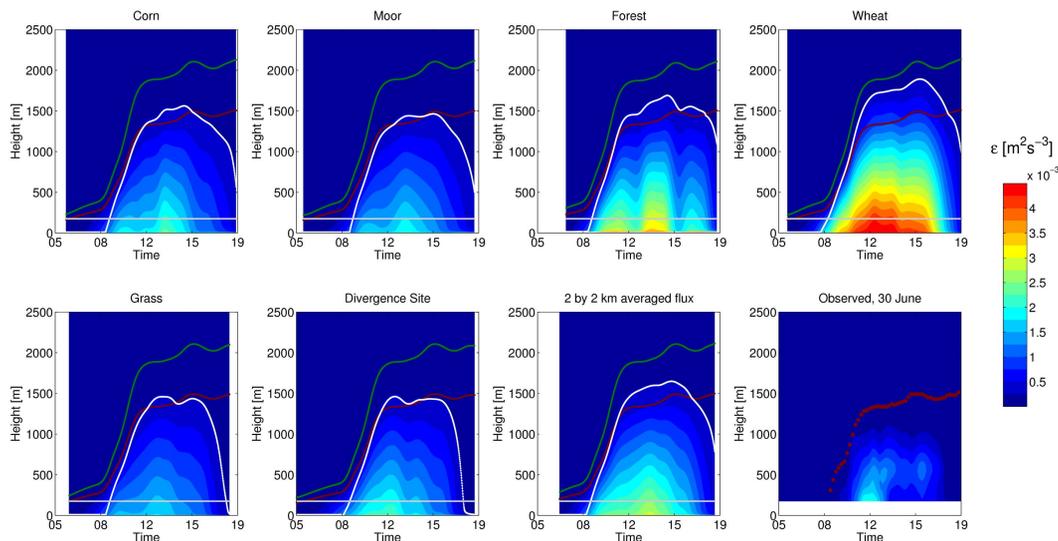
Figure 11. Modeled boundary layer dissipation rate for 30 June for six simulations over different surfaces with available near-surface measurements during the BLLAST field campaign, as well as a simulation driven by a 2 km × 2 km averaged flux. The lower right figure shows the observed dissipation rate from the UHF wind profiler between 175 and 2000 m. The red line or dots indicate model and observed boundary layer depth, green line the model height of no turbulence and an iso-line for TKE equal to $0.3 \, \mathrm{m^2 \, s^{-2}}$ is included as a white line. A horizontal gray line is also included at 175 m to show the lowest level available from the UHF wind profiler. The strong observed fluxes over forest and wheat lead to stronger TKE and dissipation rate in the simulated boundary layer, whereas the weaker fluxes over moor, corn, grass and the Divergence site yield levels of dissipation rate closer to the observed.
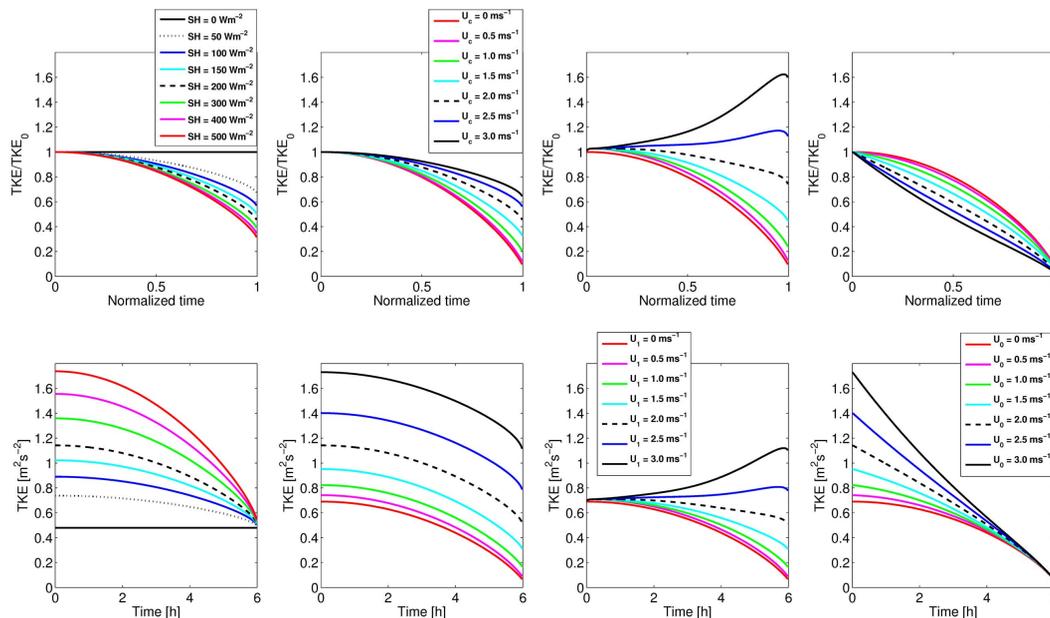
Figure 12. The lower row shows the evolution of modeled TKE at 2 m for the afternoon period in four sets of numerical simulations. In the upper row, the same simulation results are shown after dividing the TKE with the midday TKE value for each simulation and normalizing time with the length of the afternoon (here 6 h). From left to right the simulation results shown are from the SH, U_c, U_{inc} and U_{dec} numerical experiments and the legends show the relevant variable value set for each simulation. The shown legends applies to both upper and lower figures.
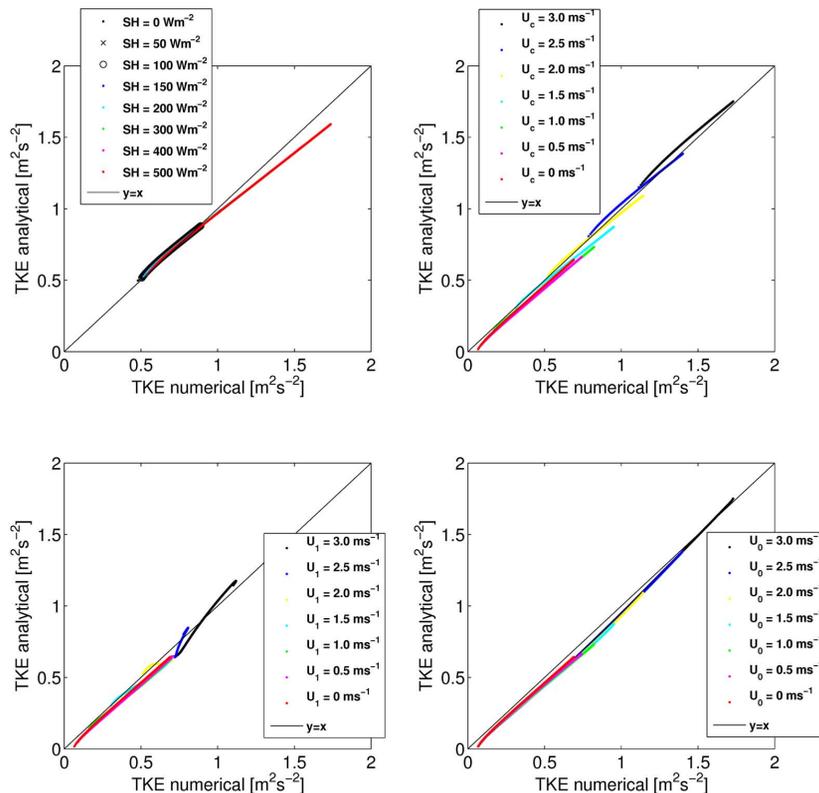
Figure 13. The figure is showing a comparison between the numerically modeled TKE and the simplified analytical quasi-stationary expression of Eq. (20). The numerical model simulations correspond to those shown in Fig. 12 with SH runs shown in upper left, U_c runs in upper right, U_{inc} in lower left and U_{dec} runs in lower right. Each simulation is identified in the legend of each figure by its set variable value.

Title Page

Abstract | Introduction

Conclusions | References

Tables | Figures

|◀ | ▶|

◀ | ▶

Back | Close

Full Screen / Esc

Printer-friendly Version

Interactive Discussion
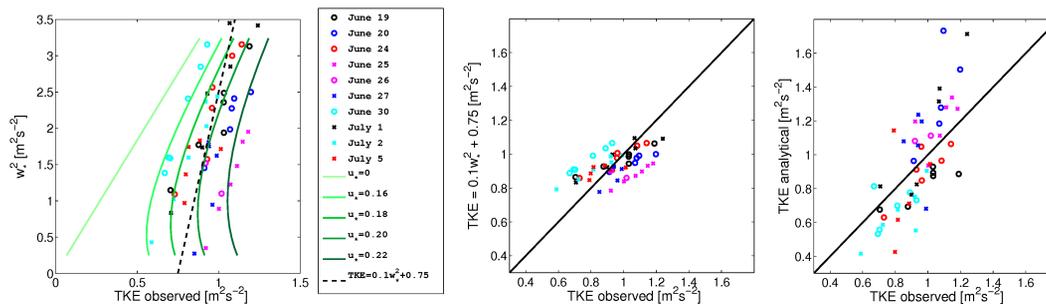
Figure 14. (Left panel) Observed w_*^2 as a function of observed TKE using hourly afternoon data. Here, Eq. (20) is illustrated with green colored lines for five different values of u_* and $z_i = 750$ m. A dashed black line is also shown as a fit to all the data. The hourly data have been assigned different colored symbols for different days as described in the legend and the same symbols are used in the middle and right panels. (Middle panel) TKE calculated from the simple linear fit plotted as a function of the observed TKE. (Right panel) TKE estimated from Eq. (20) plotted against observed TKE. Here, the observed u_*, z_i and w_* values have been used together with Eq. (20).
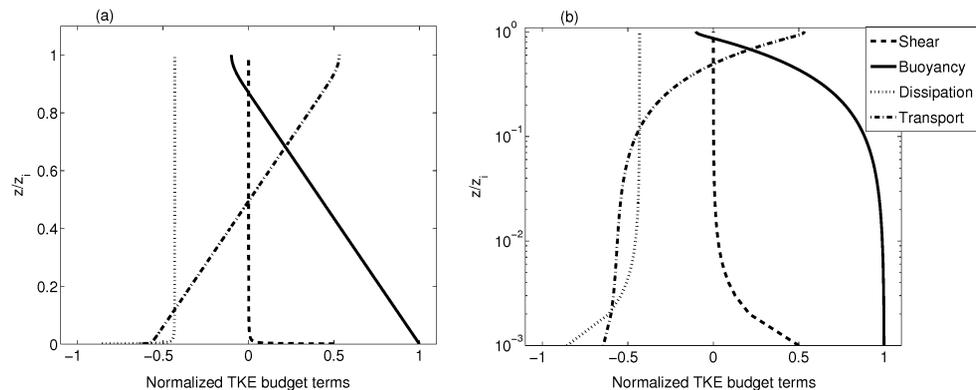
Figure A1. Normalized terms in the turbulence kinetic energy equation from Lenschow (1974) for a convective case with z_i/L equal to -1000, $z_i = 1000$ m and a surface roughness length $z_0 = 0.02$ m. Buoyancy production, shear production, dissipation and transport is shown with full, dashed, dotted and dash-dotted lines respectively for normalized height z/z_i in panel **(a)** and with a logarithmic y axis in panel **(b)**.
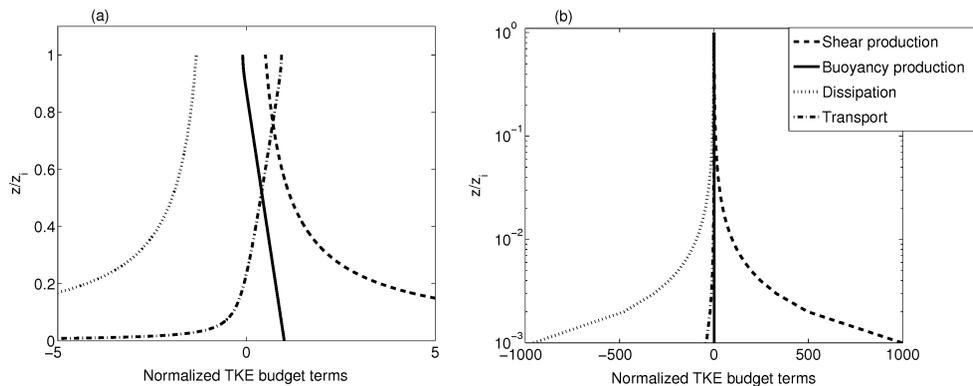
Figure A2. Normalized terms in the turbulence kinetic energy equation from Lenschow (1974) for a very near neutral case with z_i/L equal to -1, $z_i = 1000$ m and a surface roughness length $z_0 = 0.02$ m. Buoyancy production, shear production, dissipation and transport is shown with full, dashed, dotted and dash-dotted lines respectively for normalized height z/z_i in panel **(a)** and with a logarithmic y axis in panel **(b)**.